AD-A048 473 GEORGIA INST OF TECH ATLANTA ENGINEERING EXPERIMENT --ETC F/G 17/9
ENVIRONMENT AND RADAR OPERATION SIMULATOR.(U)
AUG 77 S N COLE, A R CLAYTON, E R FLYNT DAAB07-74-C-0272
UNCLASSIFIED ECOM-74-0272-F NL

1 OF 1
ADA048473

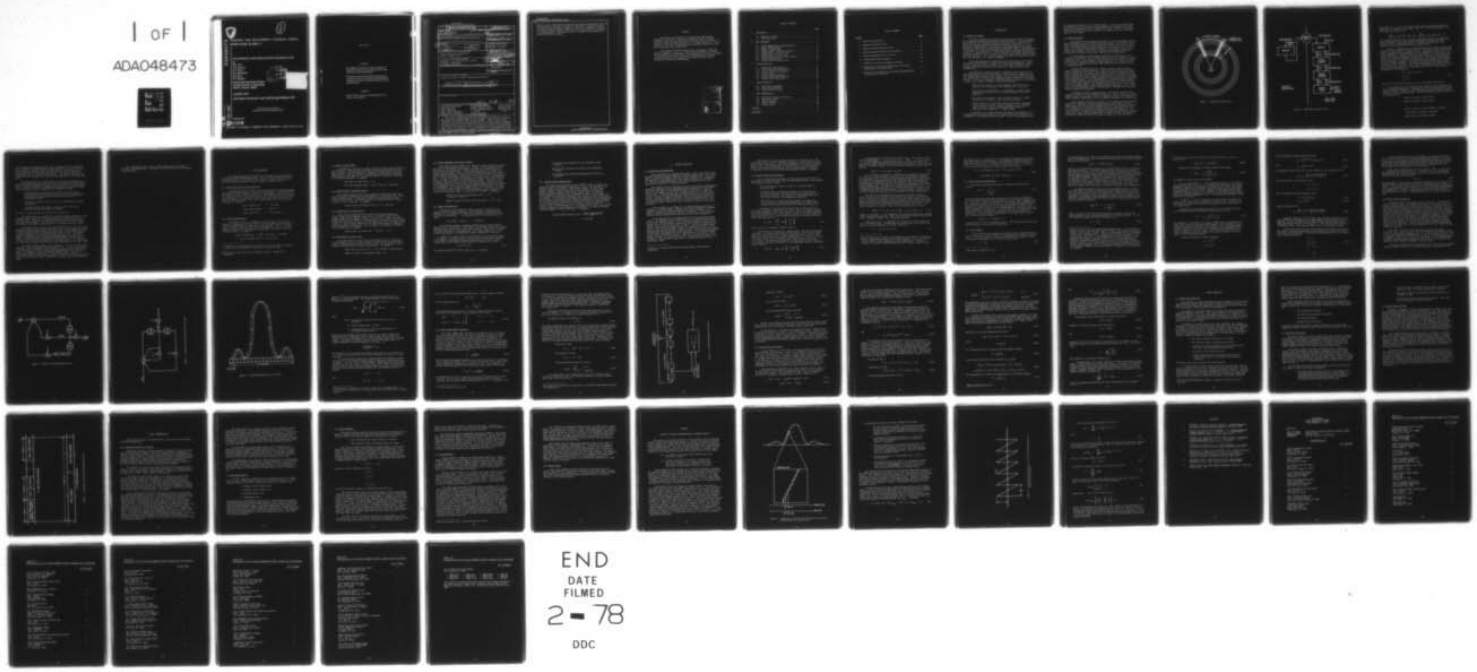

END
DATE FILMED
2-78
DDC

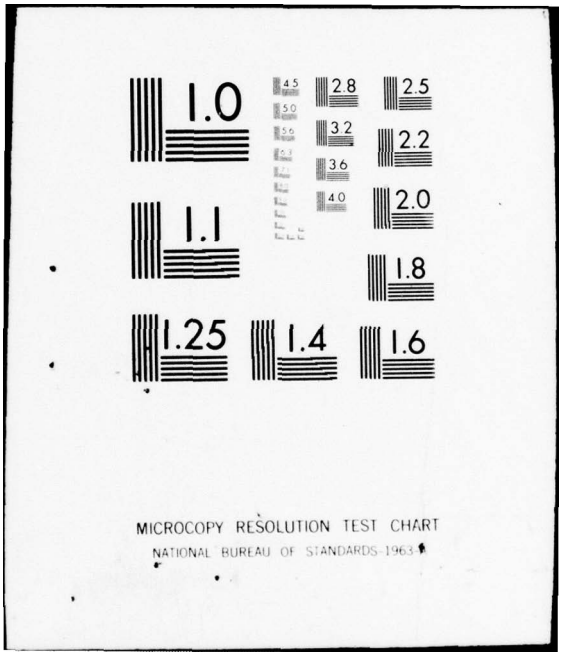
1.0
1.1
1.25
1.4
1.6
1.8
2.0
2.2
2.5
2.8
3.2
3.6
4.0
4.5
5.0
5.6
6.3
MICROCOPY RESOLUTION TEST CHART
NATIONAL BUREAU OF STANDARDS-1963-A

# RESEARCH AND DEVELOPMENT TECHNICAL REPORT

## REPORT ECOM–74–0272–F

# ENVIRONMENT AND RADAR OPERATION SIMULATOR

By
S.N. Cole
A.R. Clayton
E.R. Flynt
R.C. Michelson
B.S. Rice
E.S. Sjoberg

Engineering Experiment Station
Georgia Institute of Technology
Atlanta, Georgia 30332



AUGUST 1977

Final Report for Period 21 June 1974 through 30 March 1977





Prepared for

ECOM

US ARMY ELECTRONICS COMMAND FORT MONMOUTH, NEW JERSEY 07703

# NOTICES

## Disclaimers

The findings in this report are not to be construed as an official Department of the Army position, unless so designated by other authorized documents.

The citation of trade names and names of manufacturers in this report is not to be construed as official Government indorsement or approval of commercial products or services referenced herein.

## Disposition

Destroy this report when it is no longer needed. Do not return it to the originator.

UNCLASSIFIED

SECURITY CLASSIFICATION OF THIS PAGE *(When Data Entered)*

## REPORT DOCUMENTATION PAGE

READ INSTRUCTIONS BEFORE COMPLETING FORM

1. REPORT NUMBER: ECOM-74-0272-F
2. GOVT ACCESSION NO.
3. RECIPIENT'S CATALOG NUMBER
4. TITLE *(and Subtitle)*: ENVIRONMENT AND RADAR OPERATION SIMULATOR.
5. TYPE OF REPORT & PERIOD COVERED: FINAL rept. 21 Jun 74 - 30 Mar 77
6. PERFORMING ORG. REPORT NUMBER
7. AUTHOR(s): S. N. Cole, A. R. Clayton, E. R. Flynt, R. C. Michelson, B. S. Rice, E. S. Sjoberg
8. CONTRACT OR GRANT NUMBER(s): DAAB07-74-C-0272
9. PERFORMING ORGANIZATION NAME AND ADDRESS: Georgia Institute of Technology, Atlanta, Georgia 30332
10. PROGRAM ELEMENT, PROJECT, TASK AREA & WORK UNIT NUMBERS: ~~DA Proj~~ C8-3-05107-05-C8-CA; ~~AMC Proj~~ 1S7-62703-D-H93-P1-06; AMC Code ~~672703.12.H93.P1.06~~
11. CONTROLLING OFFICE NAME AND ADDRESS: Commander, U.S. Army Electronics Command, Attention: DRSEL-CT-R, Ft. Monmouth, NJ 07703
12. REPORT DATE: Aug [redacted] 77
13. NUMBER OF PAGES: 45 (12) 52p.
14. MONITORING AGENCY NAME & ADDRESS *(if different from Controlling Office)*
15. SECURITY CLASS. *(of this report)*: UNCLASSIFIED
15a. DECLASSIFICATION/DOWNGRADING SCHEDULE
16. DISTRIBUTION STATEMENT *(of this Report)*: Approved for public release; distribution unlimited.

(16) 1S762703D H93 (17) P1

17. DISTRIBUTION STATEMENT *(of the abstract entered in Block 20, if different from Report)*
18. SUPPLEMENTARY NOTES

153 850

19. KEY WORDS *(Continue on reverse side if necessary and identify by block number)*

| | | |
|---|---|---|
| Environment Simulation | Pseudo-Random Numbers | Complex Envelope |
| Signal Synthesis | Discrete Random Process | Digital Filter |
| Radar Simulation | Clutter Amplitude Distribution | Real-Time Simulation |
| Radar Target Simulation | Clutter Spectrum | |
| Radar Clutter Simulation | | |

20. ABSTRACT *(Continue on reverse side if necessary and identify by block number)*

This report summarizes activities performed under contract to the U.S. Army Electronics Command (ECOM) for the purpose of designing and building an Environment and Radar Operation Simulator (EROS). EROS is electrically connected to the subject radar and simulates the external world by producing synthetic backscatter from targets and clutter in a battlefield environment. Its purpose is to reduce the cost of environment testing by improving repeatability and controllability of test conditions and by replacing some of the field testing with laboratory testing. Clutter is synthesized by an array of →

DD FORM 1 JAN 73 1473 EDITION OF 1 NOV 65 IS OBSOLETE

UNCLASSIFIED

SECURITY CLASSIFICATION OF THIS PAGE *(When Data Entered)*

digital filters, which provide controllable amplitude distributions, spatial distributions, and spectra. Targets are simulated by combining recorded backscatter with user-defined maneuvers. The major components of EROS are a programmed digital computer, special-purpose high speed digital hardware, and analog hardware. The outputs consist of simulated video signals and range-gated Doppler signals.

## PREFACE

This report was prepared at the Georgia Tech Engineering Experiment Station under Contract No. DAAB07-74-C-0272. The work covered by this report was performed in the Radar and Instrumentation Laboratory under the supervision of Dr. E. K. Reedy and Mr. J. L. Eaves, Director of the Radar and Instrumentation Laboratory and Chief of the Radar Technology Area, respectively.

This project has been monitored by Mr. Reinhard G. Olesch and Mr. Otto Rittenbach of the U. S. Army Electronics Command, and their helpful guidance is acknowledged. The contributions of Dr. R. W. Schafer of the Georgia Tech School of Electrical Engineering have provided excellent guidance in the design of the digital filters, and his assistance is gratefully acknowledged.

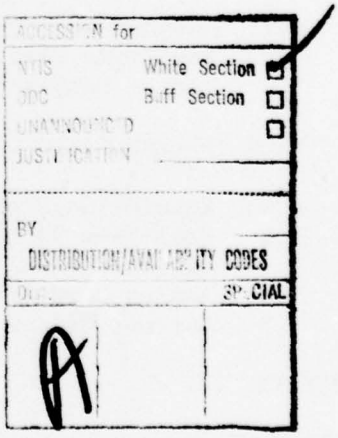

TABLE OF CONTENTS

LIST OF FIGURES

# 1. INTRODUCTION

## 1.1 Purpose of Program

This report describes the technical objectives and reviews the research and development performed under Contract DAAB07-74-C-0272. The project began on 21 June 1974 and has been sponsored by the Radar Technical Area of the Combat Surveillance and Target Acquisition Laboratory within the U. S. Army Electronics Command (ECOM). The purpose of the program has been to design and build an Environment and Radar Operation Simulator (EROS). EROS synthesizes controllable radar backscatter combining realistically simulated returns from a variety of targets and clutter. This backscatter incorporates amplitude and frequency fluctuations due to variations in radar cross section, Doppler shifts, and other phenomena. The resulting synthetic waveform is available for insertion into the radar at IF, video, and Doppler.

The simulated scenario is specified by the EROS operator and includes the locations and movements of objects producing radar backscatter: troops, vehicles, vegetation, hills, insects, etc. The scenario description also includes radar and reflectivity characteristics: antenna pattern, range dependence, etc.

The EROS system translates scenario information into signal data in a form appropriate for real-time simulation. During real-time simulation, the EROS system combines scenario data, signals from the subject radar, and operator commands into realistic radar backscatter, which is applied to the radar receiver. This form of simulation permits laboratory testing as an alternative to field testing and has a number of potential advantages:

- EROS testing promises to be less expensive than field testing, because of the convenience of the laboratory as a test site.
- The results are controllable to a high degree of scenario detail. Unpredictable influences such as weather changes do not affect EROS tests.
- The tests are repeatable. This has obvious benefits in experimentation and in repair of radar receiver components.
- Signal insertion at frequencies other than RF permits simulated field testing of specific receiver components (e.g., embodying unproven clutter reduction techniques) without having to incorporate this component in a complete radar.

In principle, it is highly desirable for EROS to be applicable to all existing troop surveillance radars and to embody sufficient flexibility to accommodate as yet unspecified radar designs. This is a long-range goal and

not a specific objective of the current program. A particular subject radar, the AN/PPS-15, has been chosen to prove feasibility of the EROS concept and design, and EROS has been built to address this radar. However, the design incorporates flexibility that will permit easy adaptation of the first EROS system to other radars.

## 1.2 EROS Description

The scenario to be simulated (see Figure 1) is an annular shaped region, which represents the portion of the battlefield visible to the radar. The region is subdivided into concentric rings (at constant range from the subject radar) and radial columns (at constant azimuth with reference to the subject radar). The simulated antenna beam consists of a contiguous subset of m of these azimuth columns. The center of the beam is determined by sampling a voltage from the subject radar, which represents its antenna angle.

The intersection of range rings and azimuth columns defines a subdivision of the scenario into four-sided cells, which will hereafter be called "simulation cells." The concept of the simulation cell is useful in providing a reference for the EROS operator in defining the scenario. Moreover, much of the internal communication between EROS components is expressed in terms of simulation cells.

The EROS hardware consists of a digital computer, special purpose digital hardware, and analog hardware. The flow of data between these components is illustrated in Figure 2. The computer contains a cathode ray tube graphic display unit and approximately 40 million bits of online disk storage. These facilities are used to assist the EROS operator in defining the scenario and to participate in the real-time simulation by supplying control information to the digital hardware. The digital hardware, in turn, generates synthetic clutter backscatter, applies antenna pattern weighting, and combines clutter signals with target signals. The combined data are sent to the analog hardware. The analog hardware applies range-dependent weighting (e.g., $R^{-4}$ power attenuation) and generates a video frequency signal incorporating the subject radar's transmitter modulations.

The target and clutter signals reflect the Doppler and radar cross section fluctuations of the simulated backscatter. In the computer and digital hardware these are expressed in terms of sampled waveforms. Each sample is a complex quantity represented by the two quadrature components of the waveform.

Target signals in EROS are recorded on the computer disk during scenario definition. Additional target data (specified via the computer's graphic display unit) consists of target-movement definition and a schedule of events. This information is compiled onto a disk file and is subsequently retrieved for transmission to the digital hardware during real-time simulation. To ensure realism, the target signal strength is apportioned between two adjacent range rings. More precisely, assume that the target's signal strength is s and that the target is between the center of range ring r and the center of

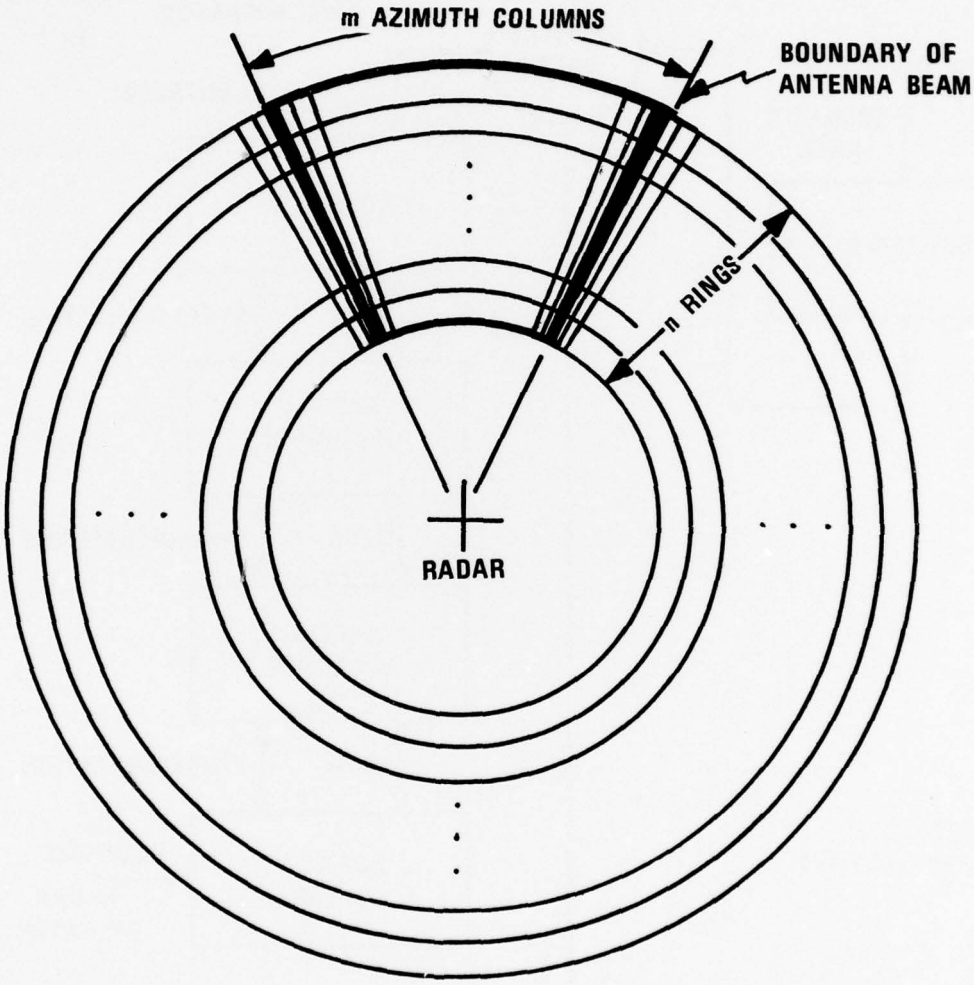


Figure 1. Simulated Coverage Area.

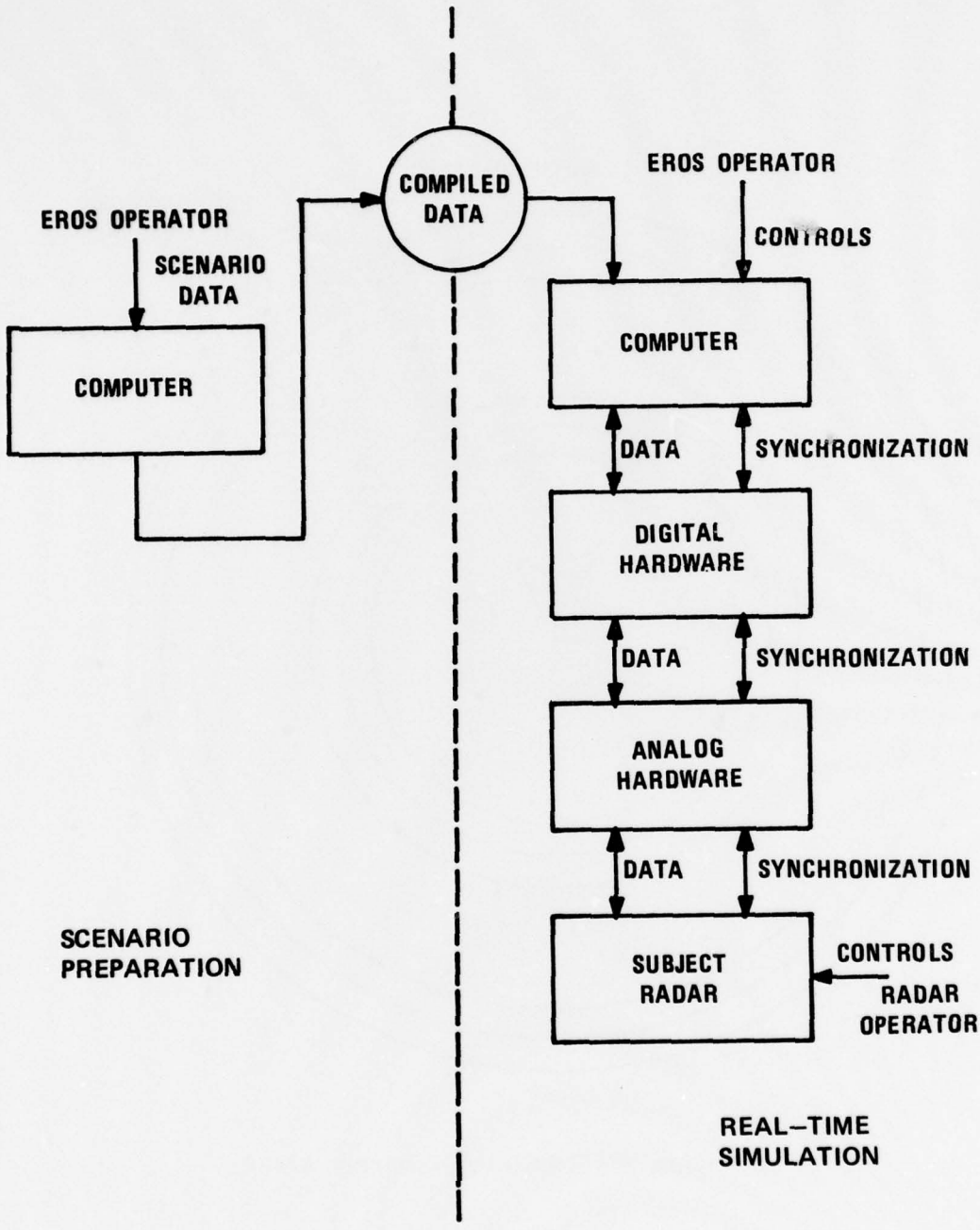


Figure 2. EROS Data and Control Flow.

range ring r + 1. Let $d_0$ and $d_1$ denote the respective distances between the target and the centers of range rings r and r + 1. Then the backscatter from the target is represented as

$$\frac{d_1 s}{d_0 + d_1} \text{ from range ring r and } \frac{d_0 s}{d_0 + d_1} \text{ from range ring r + 1.}$$

The reason for doing this is to avoid an abrupt discontinuity (in range-gated radar reception) as the target crosses the boundary between range rings. A similar problem in azimuth boundaries is avoided by utilizing very high resolution in the representation of the antenna pattern.

Clutter is synthesized in the digital hardware by applying pseudo-random sequences (digital noise) to digital filters. The outputs from the filters have spectra and amplitude distributions that are controllable as functions of the filter parameters. Clutter backscatter is represented as the sum of the radar returns from moving scatterers (e.g., foliage, insects, etc.) and fixed scatterers (e.g., ground, buildings, boulders, etc.). The return from the moving portion of clutter is created by two identical 2-pole filters, which generate the two quadrature components. The return from the fixed portion of clutter is simply a complex constant. The 2-pole filter employs two feedback multipliers $\alpha_1$ and $\alpha_2$. The state of the filter is defined by the most recent output $w_1$ and the previous output $w_2$. The transition to the next filter state is described by the computation:

$$\begin{aligned} w' &\leftarrow \alpha_1 w_1 + \alpha_2 w_2 + x \\ w_2 &\leftarrow w_1 \\ w_1 &\leftarrow w' \end{aligned} \qquad (1\text{-}1)$$

where w' is the next filter output, and x is the pseudo-random input.

The computations are performed by two identical units of hardware for the two quadrature components. The parameters and state information are maintained in read-write memory--the memory holds one set of such data for each simulation cell in the antenna beam. The filter hardware performs computations in an endless loop:

```
update the state of filter number 1
update the state of filter number 2
. . .
update the state of filter number k (k denotes
  the number of filters in the beam)
update the state of filter number 1
. . .
```

This arrangement avoids maintaining k sets of hardware for the k simulation cells. Moreover, by permitting the digital computer to write into the parameter memory, it provides a means for simulating the clutter response to antenna scanning. As simulation cells drop off the trailing edge of the antenna beam, new cells enter the leading edge. The computer overwrites the parameters of the trailing-edge cells with the parameters of the leading-edge cells.

One loop through the k cells constitutes one Doppler sampling cycle. The clutter hardware produces samples for k cells during the Doppler sampling cycle. These are combined with a small number (at most two) of target-signal samples with their respective antenna-pattern weights and range ring numbers that the computer has sent. These data are combined as follows:

- Azimuth weights are applied to the target and clutter samples (the antenna pattern for clutter is sent from the computer during initialization and the digital hardware stores this array in a random-access memory).
- All clutter samples at the same range are added together (azimuth integration).
- The target samples are added to the appropriate clutter sums (based on the specified range-ring number).

The result is range profile--one value for each range ring.

The range profile is recomputed at the Doppler sampling frequency, which is several times slower than the pulse-repetition frequency (PRF) of the AN/PPS-15 radar. Therefore, the digital hardware stores each range profile in a random-access memory. This same data is retrieved at the PRF; several repetitions of the same data are used before a new range profile is stored.

The range profile is sent to the analog hardware at the PRF. Each transmission is delayed a fixed interval after the radar's pulse trigger; this delay corresponds to the distance between the radar and the closest simulated range. The range samples are sent in ascending range order. The interval between samples corresponds to the width of the simulated range ring. Each range sample is accompanied by the corresponding range-dependent attenuation. For example, the range attenuation might vary proportionally to $R^{-2}$ to simulate $R^{-4}$ power loss. After the transmission of the range sample for the most distant ring, the digital hardware waits for the trigger denoting the next radar pulse.

The analog hardware employs 3 D/A converters: 1 for the in-phase signal component, 1 for the quadrature signal component, and 1 for the range weight. The range weight is applied to the two signal components using an analog multiplier. The signals are then fed through an analog integrator in order to simulate the transmitter modulation of the AN/PPS-15 radar. Finally, a controllable amount of analog noise is added to account for antenna and receiver-front-end noise, and the result is applied to the video stage of the AN/PPS-15 radar.

The remaining sections of this report explore some of the theory developed in the EROS design. Also much of the above description is repeated in greater detail.

## 2. EROS PARAMETERS

This section summarizes decisions that were made concerning parameters for the first EROS implementation model. Many of these parameters are based on characteristics of the AN/PPS-15 radar, and they should be reviewed carefully when considering EROS revisions to address a different radar.

### 2.1 Video Sampling Rate--Range Resolution

The video sampling rate refers to the transmission of range-ring samples from the EROS digital hardware to the EROS analog hardware. This rate must be fast enough to yield a range of resolution of approximately 15 meters, one-half the range resolution of the AN/PPS-15 radar.* The sampling rate is also chosen for convenience to be a multiple of the 37.5 KHz rate of the AN/PPS-15 transmitter's modulator trigger. The value selected equals (266) x (37.5 KHz) or 9.975 MHz. In summary:

Video sampling rate = 9.975 MHz

Video sampling period = 100.25 ns

Range ring width** = 15.027 meters.

### 2.2 Doppler Sampling Rate

The AN/PPS-15 radar has a Doppler cut-off frequency of about 1 KHz. Therefore, a sampling rate on the order of 4 KHz is judged to be adequate for faithful representation of target and clutter envelopes. Since it is convenient to choose the sampling rate to be an integral divisor of the 37.5 KHz modulator trigger rate, the sampling frequency $(\frac{1}{9})$ x (37.5 KHz) $\doteq$ 4.167 KHz has been selected. In summary:

Doppler sampling rate = $(\frac{1}{9})$ x (37.5 KHz) $\doteq$ 4.167 KHz

T = Doppler sampling period = 240 μseconds.

---

*A sampling rate corresponding to the 30 meter range resolution is inadequate because of the representation of targets in two adjacent rings.

**This value is based on the radar propagation speed of $2.99796 \times 10^8$ meters/sec.

## 2.3 Number of Range Rings

The AN/PPS-15 is sensitive to radar return from ranges between 50 meters and 3000 meters. Simulating this 2950 meter range would require 190 15-meter rings. However, it is not necessary to simulate the entire range in any one simulation run. EROS will provide the capability of simulating 64 contiguous rings during any one simulation run, and the specific 64 rings are selectable as a simulation parameter. In summary:

The number of range rings = 64

The total simulated range $\doteq$ (64) x (15.027) $\doteq$ 962 meters.

## 2.4 Azimuth Width of Simulated Clutter

The azimuth antenna pattern for the AN/PPS-15 indicates that the null following the first sidelobe occurs approximately 11° from center beam. Therefore, a simulated area 22° wide would include the main beam and the first sidelobe on both edges. A convenient width for the EROS simulation is $\frac{1}{16}$ of a circle = 22.5° = 400 mils. In summary:

Azimuth width of simulated clutter = 22.5° = 400 mils.

## 2.5 Azimuth Width of Clutter Cells

The azimuth column width in the scenario partition determines the azimuth width of each simulated clutter cell. A convenient value for the azimuth column width is $\frac{1}{256}$ of a circle = 25 mils $\doteq$ 1.4°. Since the azimuth antenna pattern for the AN/PPS-15 indicates that the main beam is about 6° wide between the 3 dB points and about 13° wide between the nulls, this would provide at least 4 azimuth columns between the 3 dB points and at least 9 azimuth columns between the main-beam nulls. This is judged to be adequate for realistic clutter simulation. In summary:

Azimuth width of clutter cell = 25 mils $\doteq$ 1.4°.

## 2.6 Range Width of Clutter Cells

The range width of clutter cells has been chosen to be 2 range rings or approximately 30 meters. This provides 32 clutter cells for each azimuth column. Subdividing the simulated clutter scenario into 32 30-meter rings is judged to provide adequate realism and flexibility. In summary:

Range width of clutter cell $\doteq$ (2) x (15.027) = 30.054 meters

Number of clutter cells/azimuth column = 32.

## 2.7 Azimuth Dependence Upon Target Samples

The antenna pattern weights to be applied to target samples are stored in a table in the computer's main memory. Because of real-time constraints, this table is not interpolated; instead, the entry that corresponds to the closest target azimuth is used. If the azimuth spacing is too coarse, the antenna gain will remain constant for several Doppler sampling cycles and then undergo a jump discontinuity. Repetition of this behavior at low frequencies will introduce an annoying spurious tone in the aural output of the AN/PPS-15 radar. A study was performed to determine how frequently the antenna pattern gain must change in order to avoid this spurious signal. The result is that the antenna gain must change at least 1244 times/second to reduce the worst-case spurious signal to 72 dB below the saturating signal (details are supplied in the Appendix). This constraint coupled with the 90 mils/second scan rate of the AN/PPS-15 radar implies an azimuth spacing of $2^{-17}$ circles. The width of the antenna pattern is $\frac{1}{16}$ of a circle, and pattern symmetry implies that only half of the pattern needs to be repeated in the table. In summary:

Azimuth spacing of antenna-pattern table = $2^{-17}$ circles $\doteq$ .00275°

Number of points in pattern table ($\frac{1}{2}$ pattern) = $2^{12} = 4096$

## 2.8 Sample Representation

Target and clutter signals are represented by bit patterns in the computer and in the digital hardware. Two's complement representation is employed, and the quantities are generally interpreted as binary fractions. Thus the bit pattern $b_0 b_1 \ldots b_m$ ($b_k$ equals 0 or 1) is interpreted as the value

$$-b_0 + (\tfrac{1}{2})\, b_1 + (\tfrac{1}{4})\, b_2 + \ldots + (\tfrac{1}{2})^m\, b_m.$$

The interface between the digital hardware and the analog hardware employs 12-bit D/A converters. This permits 72 dB dynamic range in the signal amplitude due to Radar Cross Section (RCS) variation. (Note that the additional dynamic range due to range dependence is not constrained by this choice, because range weights are transmitted through a separate D/A converter.)

The RCS $\sigma$ of a signal sample is proportional to the squared amplitude of the sample. The values I and Q of the in-phase and quadrature components of the sample are determined by using the binary-fraction interpretation stated above, and the proportionality constant is denoted by $K_\sigma$. Thus,

$$\sigma = K_\sigma\, (I^2 + Q^2) \qquad (2\text{-}1)$$

The constant 20,000 $m^2$ has been chosen for $K_\sigma$. In summary,

Bit patterns are interpreted as 2's complement binary fractions.

Twelve-bit D/A converters are used for each quadrature component.

The proportionality between squared amplitude and RCS is 20,000 $m^2$.

## 2.9 Antenna Azimuth Sampling Rate

The antenna azimuth accuracy of the AN/PPS-15 radar is judged to be roughly the same as the read-out resolution, 5 mils. The scan rate of the AN/PPS-15 radar is 90 mils/sec. EROS selects samples from the antenna azimuth voltage at about the same rate as the frequency at which the AN/PPS-15 azimuth changes by the accuracy amount, 90/5 ≈ 18 times/sec. Between samples the azimuth value is computed by linear interpolation. If the azimuth were sampled less frequently, the azimuth accuracy of EROS would be degraded. If the azimuth were sampled more frequently, the discontinuities due to accuracy limitations in the azimuth voltage would be more pronounced. The possible adverse consequences of the latter problem are spurious signals at the azimuth sampling rate, an effect similar to that described in Section 2.7 due to discontinuities in the antenna-pattern table. The azimuth sampling frequency has been chosen for convenience to be 1/256 the Doppler sampling frequency or about 16.28 Hertz. In summary

$$\text{Antenna azimuth sampling rate} = \frac{\text{Doppler Sampling Rate}}{256}$$

$$= 16.28 \text{ Hertz} \quad .$$

# 3. CLUTTER SIMULATION

## 3.1 Backscatter Representation

Radar backscatter is a modulated RF signal. Radar cross section fluctuations introduce amplitude modulations, and the Doppler shifts due to movements of reflecting elements constitute frequency modulations. In general, the bandwidth of this modulation is very narrow compared to the transmitted RF. This narrow bandwidth permits a much simpler representation of the backscatter in terms of its complex envelope.*

The complex envelope, expressed in terms of the in-phase component and quadrature component, is the radar backscatter representation used in EROS. Since the video signal of the AN/PPS-15 radar is produced by a coherent detector, the complex envelope can be applied directly to the video stage of the radar. For radars employing non-coherent detectors it would not be correct to apply the complex envelope at video without additional EROS processing. Instead it might be necessary to create a modulated signal from the synthetic envelope and either (1) to insert this as RF or IF, or (2) to replicate the radar's detector in order to insert the detected signal into the radar.

To be realistic, the envelope of the radar backscatter should be represented as a random process. However, since EROS is designed to produce repeatable results, the simulated backscatter envelope cannot be truly random. Nevertheless, EROS does produce a facsimile of a typical waveform selected from the random process specified by the scenario parameters.

The characteristics of a random process are often expressed statistically. Two commonly cited characteristics are the amplitude distribution and the power spectral density. For a stationary continuous-valued random process $x(t)$, the amplitude distribution is the probability distribution of $|x(t_0)|$, where $t_0$ is any fixed value of time t. The power spectral density of $x(t)$ is the Fourier transform of the auto-correlation function of $x(t)$. (Refer to [1]). The clutter model in EROS is a random process with controllable amplitude distribution and power spectral density. The underlying assumption of this model--that backscatter can be represented as a stationary random process--is not necessarily correct. There is a risk that the use of stationary statistics to describe clutter will detract from the realism of the simulation. This question, among others, is necessarily deferred to an evaluation of EROS.

---

*Section 4 of the First EROS Quarterly Report gives a more detailed discussion.

EROS hardware produces synthetic backscatter in digital form. This is satisfactory as long as the sampling frequency is several times the bandwidth of the random process. The carrier frequency of the AN/PPS-15 radar is about 10 GHz. Since the bandwidth of X-band clutter is at most hundreds of Hertz, and since EROS simulation will restrict target Doppler frequencies to less than 1 KHz, the 4.167 KHz Doppler sampling frequency is adequate.

## 3.2 Clutter Amplitude Distribution

Of the various models available that describe clutter amplitude distributions, the Ricean has been chosen for EROS implementation. This decision was prompted by several factors:

- The Ricean density function is based on a physical model of ground clutter.
- The Ricean model has widespread support in the literature as a realistic amplitude distribution model for ground clutter. It has been successfully curve-fitted to clutter measurement data taken under a variety of environmental conditions.
- The assumption of a Ricean amplitude distribution makes the clutter synthesis implementation manageable. The SAM-D project incorporates a Ricean clutter model in its radar simulator [2].

A derivation of the Ricean distribution from a physical model of clutter is provided by Goldstein [3] in which a signal is formed by adding two signal components. The complex envelope of one of the signal components has a constant magnitude $|S|$. The complex envelope of the other signal component fluctuates with a uniform phase distribution and a Rayleigh distribution of the amplitude $|R|$:

$$W_1(|R|) = \frac{2|R|}{P_0} \exp\left(-\frac{|R|^2}{P_0}\right) \tag{3-1}$$

where $W_1$ denotes a probability density function.

The technique for generating a random process with a Ricean amplitude distribution is based on Goldstein's physical model: the sum of two signal components, one of which has a constant complex envelope S, and the other, which is a random process with complex envelope R(t), is described as follows. The random process R(t) is stationary with complex values of the form $X(t) + jY(t)$. The probability distribution of $R(t_0)$ for any fixed time $t_0$ is a bivariate Gaussian distribution of the random phasor $X(t_0) + jY(t_0)$ with density function

$$W_1(X,Y) = \frac{1}{\pi P_0} \exp\left(-\frac{X^2 + Y^2}{P_0}\right). \tag{3-2}$$

The implementation parallels this physical model. Two series of independent random samples . . . $u_{-1}$, $u_0$, $u_1$, $u_2$, . . . and . . . $v_{-1}$, $v_0$, $v_1$, $v_2$, . . . are fed through two identical real discrete filters resulting in two real discrete random processes $Y_I(nT)$ and $Y_Q(nT)$, respectively. These are then added to the complex constant A to form the discrete complex envelope N(nT) of clutter:

$$N(nT) = A + Y_I(nT) + jY_Q(nT) . \qquad (3\text{-}3)$$

It is difficult, in general, to determine the probability distribution of $Y_I$ and $Y_Q$. In the particular case when $u_i$ and $v_i$ are Gaussian samples, it can be proven that $Y_I$ and $Y_Q$ are also Gaussian distributed.* Results show that these filter output statistics remain Gaussian under considerably wider circumstances. Experiments with filters typical of those used in EROS for clutter synthesis have indicated that the probability distribution is approximately Gaussian even if the inputs are randomly selected from the set {-1, 1}. A pseudo-random number generator with a two-point distribution is much easier to implement than one whose distribution is pseudo-Gaussian. Therefore, the two-point random number generator has been adopted for EROS implementation.

The mean of the distribution of $Y_I$ and $Y_Q$ is not zero in general (clearly $Y_I$ and $Y_Q$ are identically distributed and therefore have the same mean). This is true, in spite of the fact that the pseudo random inputs have zero mean, because of truncation errors introduced by the filter's multipliers. However, this does not increase the complexity of the filter hardware, since the non-zero bias can be compensated by the appropriate choice of A. Let $\mu$ denote the mean of $Y_I$ and $Y_Q$. Then (3-3) can be rewritten in the form

$$N(nT) = A + \mu(1 + j) + [Y_I(nT) - \mu] + j\,[Y_Q(nT) - \mu]. \qquad (3\text{-}4)$$

$Y_I(nT) - \mu$ and $Y_Q(nT) - \mu$ are independent and identically distributed Gaussian random variable with zero mean. Their bivariate density function has the form (3-2). Therefore, $|N(nT)|$ has a Ricean distribution.

The term $A + \mu(1 + j)$ represents the component of clutter backscatter due to fixed scatterers. Its amplitude should correspond to the radar cross section $\sigma_1$ of this component of clutter. From (2-1)

$$\sigma_1 = K_\sigma\, |A + \mu(1 + j)|^2 . \qquad (3\text{-}5)$$

---

*This is because $Y_I$ and $Y_Q$ can be represented as convolutions of the discrete filter's unit-impulse response with a random sequence. This convolution is, in turn, simply a linear combination of the random inputs. A linear combination of Gaussian random variables yields a Gaussian random variable.

The term $[Y_I\ (nT) - \mu] + j[Y_Q\ (nT) - \mu]$ represents the component of clutter backscatter due to moving scatterers. Its amplitude should correspond to the radar cross section $\sigma_2$ of the moving part of clutter. However, since the radar cross section from a collection of moving scatterers is not constant, $\sigma_2$ more appropriately denotes the average radar cross section.

$$\begin{aligned}\sigma_2 &= K_\sigma \text{ average } \{[Y_I\ (nT) - \mu]^2 + [Y_Q\ (nT) - \mu]^2\} \\ &= K_\sigma \text{ variance } \{Y_I\ (nT) + jY_Q\ (nT)\}\end{aligned} \tag{3-6}$$

## 3.3 Clutter Spectral Distribution

The clutter spectral model adopted for EROS is expressed by the formula*

$$P(f) = \frac{1}{1 + \left|\frac{f}{f_c}\right|^n}\ , \tag{3-7}$$

where P(f) denotes the power spectral density as a function of frequency, $f_c$ is the cutoff frequency, and n expresses the rate of high frequency roll-off. The value of n has been observed to vary between 2 and 4 depending upon the transmitter frequency and the type of clutter producing backscatter [5]. Formula (3-7) applies only to the fluctuating component of clutter. This model was derived by fitting curves to measurement data from which the 0-frequency component was filtered out. Note also that (3-7) is normalized so that radar-cross section dependence is eliminated, and P(f) approaches 1 as f approaches 0. Thus the spectral requirement for the EROS clutter model is that the power spectral density of

$$[Y_I(nT) - \mu] + j[Y_Q(nT) - \mu]$$

be proportional to P(f) as expressed in (3-7). The following sections of this report describe how this has been implemented.

## 3.4 Filter Design

It is well known that analog filters can be used to shape white noise into a signal with a desired spectrum. A similar property applies to digital filters. Let $P_x(\omega)$ denote the power spectral density of a random process x as a function of frequency $\omega$ (in units of radians/second)

$$\omega = 2\pi f\ . \tag{3-8}$$

---

*This model is suggested by [4].

If a random process x is applied to a digital filter whose unit-impulse response has the z-transform H(z), then the output random process y has the power spectral density $P_y(\omega)$ given by*

$$P_y(\omega) = |H(e^{jwt})|^2 P_x(\omega) . \qquad (3\text{-}9)$$

Equation (3-9) expresses the motivation for using digital filters to synthesize the desired spectrum. If the input random process x has an autocorrelation function with a constant value at non-0-lag and with a different value at 0-lag, then the spectrum of the input process is constant except for integer multiples of the sampling frequency. Therefore, the spectrum of the output process y is proportional to $|H(e^{jwt})|^2$ except at multiples of the sampling frequency. The sampling frequency is sufficiently high, so that the only multiple within the pass band of the subject radar is the 0-frequency term. This term represents part of the backscatter due to stationary scatterers; the constant term to be added to the filter output accounts for tne rest of this backscatter.

The approach adopted for the clutter filter design has been to select an analog filter that would provide the specified spectral shape (3-7) and to derive the digital filter from the analog filter. Consider the transfer function $H_a(s)$ of an analog filter. The spectral response of an analog filter is obtained by evaluating the squared magnitude of $H_a(s)$ along the imaginary axis. Therefore, the requirement that the analog filter have the specified spectral shape is restated in the form

$$|H_a(j\omega)|^2 \cong \frac{b}{1 + \left|\frac{f}{f_c}\right|^n} \qquad (3\text{-}10)$$

where $\omega$ is given by (3-8) and the proportionality constant b denotes the singal strength of the fluctuating component of clutter backscatter. The cut-off frequency in radians per second is denoted by $\omega_c$:

$$\omega_c = 2\pi f_c \qquad (3\text{-}11)$$

---

*Refer to Section 5.3 of the Second EROS Quarterly Report. To be perfectly accurate, the derivation in this report is inexact even though the conclusion, Formula (3-9), is still correct. Implicit in this derivation was the assumption that the z-transform of the autocorrelation function converges at all points on the unit circle. This assumption is not valid, because the input sequence has a periodic component in the form of a non-zero mean due to multiplier truncation errors (see Section 2.3 of the Sixth EROS Quarterly Report). However, if the autocorrelation function is separated into periodic and aperiodic componenets, and if the Fourier transform is applied directly to the periodic component without employing the z-transform, the result (3-9) is obtained.

By definition of the cutoff frequency, the spectral density is down by a factor of 1/2.

$$|H_a(j\omega_c)|^2 = \frac{1}{2}|H_a(0)|^2 . \tag{3-12}$$

Equation (3-10) suggests a transfer function of the form:

$$H_a(s) = \frac{b\, s_1 s_2}{(s - s_1)(s - s_2)} . \tag{3-13}$$

The reasons for this choice are as follows:

If $s_1 = \omega_c \exp(-j135°)$ -- a 2-pole Butterworth filter -- then (3-10) is satisfied exactly for the case n = 4. Moreover, a small amount of frequency aliasing is expected in the digital filter derived from (3-13). The effect would be to reduce the rate of high frequency rolloff, and it might provide an approximation for the case n= 3. Finally for some digital filter implementation a two-pole filter can be converted to a one-pole filter by setting one of the feedback multipliers to zero. A one-pole filter provides an exact solution for the case n = 2.

In order for (3-13) to correspond to a real-valued unit-impulse response, $s_1$ and $s_2$ must either be complex conjugates or real. Moreover, the filter must be stable which implies that $s_1$ and $s_2$ be in the left half of the complex plane.

Applying the impulse-invarient method [6] to the transfer function (3-12) yields a digital filter whose z-transform has the form

$$H(z) = \frac{\beta z^{-1}}{1 - \alpha_1 z^{-1} - \alpha_2 z^{-2}} . \tag{3-14}$$

The parameter $\beta$ corresponds to the signal strength and is determined by the radar cross section of the fluctuating component. The parameters $\alpha_1$ and $\alpha_2$ influence the spectral behavior of the clutter, since its simulated power spectral density (by (3-9)) will be proportional to the squared magnitude of H(z) evaluated on the unit circle. To perform such evaluations, it is useful to express $\alpha_1$ and $\alpha_2$ in terms of the cutoff frequency $\omega_c$, the pole angle $\theta$, and the sampling interval T.

If the analog poles are complex conjugates

$$s_1 = \omega_p e^{j\theta}$$

$$s_2 = \omega_p e^{-j\theta},$$

then the impulse invarient derivation yields

$$\alpha_1 = 2e^{\omega_p T \cos\theta} \cos(\omega_p T \sin\theta) \tag{3-15}$$

and

$$\alpha_2 = -e^{2\omega_p T \cos\theta}. \tag{3-16}$$

The magnitude of the pole $\omega_p$ is, in turn, related to $\omega_c$ by applying (3-12):

$$\omega_p = \omega_c \sqrt{\cos 2\theta + \sqrt{1 + \cos^2 2\theta}} \tag{3-17}$$

On the other hand, if the poles are real

$$s_1 = -\omega_p + D$$

$$s_2 = -\omega_p - D,$$

then the impulse invarient derivation yields

$$\alpha_1 = 2e^{-\omega_p T} \cosh DT \tag{3-18}$$

$$\alpha_2 = -e^{-2\omega_p T}. \tag{3-19}$$

Again by applying (3-11):

$$\omega_p = \sqrt{D^2 + \omega_c^2 + \sqrt{2\,\omega_c^4 + 4\,\omega_c^2 D^2}} \tag{3-20}$$

A graphic comparison of the filter's power spectral density with (3-7) was performed with the support of the EROS computer's graphic display unit and light pen. It was observed that pole angles between 152° and 160° provide a good approximation to (3-7) for the case n = 3. The high frequency rolloff is, as expected, closer to the desired behavior due to the frequency aliasing.

In order for a digital filter to be stable, the poles must be within the unit circle. Stability is important in this application to prevent the feedback values from overflowing. The stability condition applied to (3-14) yields the following inequalities:

$$\alpha_2 > -1$$

$$\alpha_1 + \alpha_2 < 1 \tag{3-21}$$

$$\alpha_2 - \alpha_1 < 1 \quad .$$

A more detailed analysis of filter behavior for various choices of $\alpha_1$ and $\alpha_2$ is given in Section 2.2 of the Sixth EROS Quarterly Report. Included is a map of the $(\alpha_1,\alpha_2)$ plane indicating correspondence between certain points in this plane with parameters of the analog filter (3-13) from which (3-14) was derived. Other points in the $(\alpha_1,\alpha_2)$ plane are identified with 1-pole filter behavior, which simulates (3-7) for the case n = 2.

The network corresponding to (3-14) is shown in Figure 3. The stability conditions (3-21) imply that $|\alpha_2| < 1$ and that $|\alpha_1| < 2$. Furthermore, (3-15) suggests that negative values of $\alpha_1$ will not be particularly useful. Therefore, the additional restriction

$$0 < \alpha_1 < 2 \qquad (3\text{-}22)$$

has been imposed. This permits a convenient modification of the filter to the network shown in Figure 4, which is easier to implement than the network of Figure 3. Both multipliers in Figure 4 can use the same number representation (the representation specified in Section 2.8), since the factors are restricted to magnitudes less than 1. Sixteen-bit precision has been selected to obtain sufficient resolution in representation of $\alpha_1$ of $\alpha_2$ and to avoid overflow.

## 3.5 Clutter Azimuth Weighting

The angular width of the antenna beam is identical to the width of 16 adjacent clutter columns (see Sections 2.4 and 2.5). The position of each clutter column relative to the antenna beam varies as the antenna scans. An illustration of beam scanning to the left is contained in Figure 5. The heavy curve indicates the antenna pattern relative to clutter cell positions when the pattern endpoints are exactly aligned to span 16 columns. The seventeenth column at the left end contains new filter parameters that have very recently been supplied from the EROS computer. At the time represented by the heavy curve, the 32 filters in this seventeenth column are generating samples; however, the antenna pattern above the seventeenth column is zero, which nullifies their outputs. The dashed curve in Figure 5 denotes the antenna pattern shortly thereafter. At this time the antenna pattern weighting has changed for all of the cells, and the weighting for cells in the seventeenth column is now nonzero.

The number of clutter cells simulated at any one time equals (17)x(32) = 544. Each of the 544 cells will be sampled and azimuth weighted at the 4.167 KHz Doppler sampling rate, i.e., within a period 240 μsec. These 544 weighted samples are subdivided into 32 sets of 17 samples; each set of 17 samples is taken from 17 cells at the same range. The 17 weighted samples are added together (azimuth integration), and the sum is the total clutter component of the simulated backscatter from that range.

The clutter azimuth weights are maintained in a table stored in digital-hardware random-access memory. The angular spacing between points in this

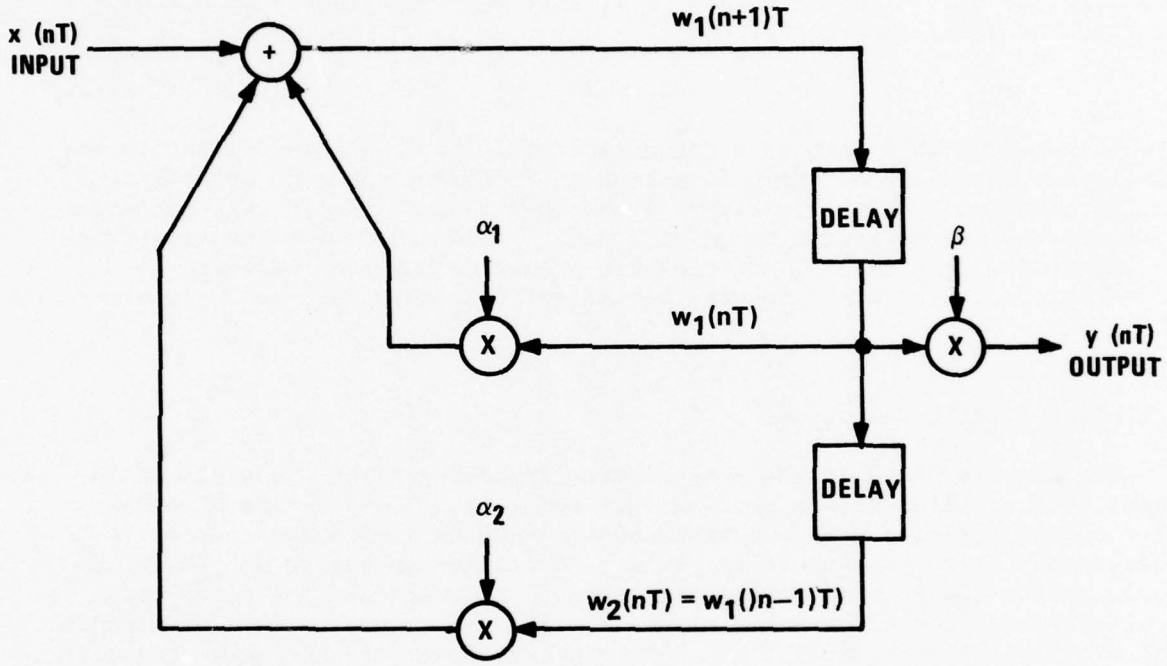


Figure 3. Network of Derived Digital Filter.

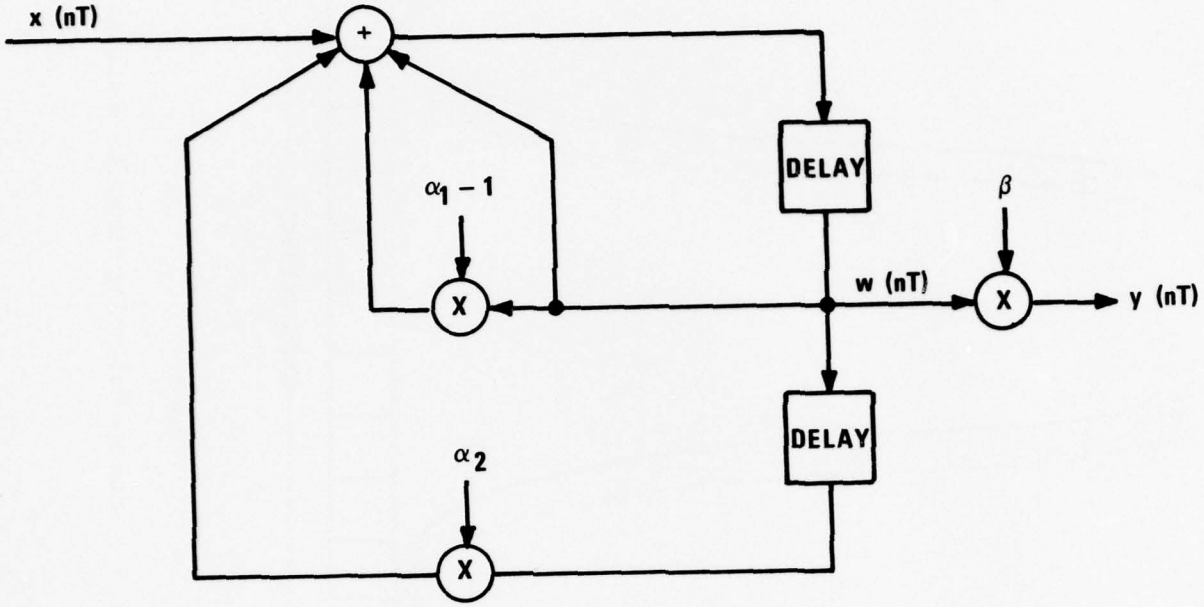


Figure 4. Modified Impulse-Invariant Filter Network.

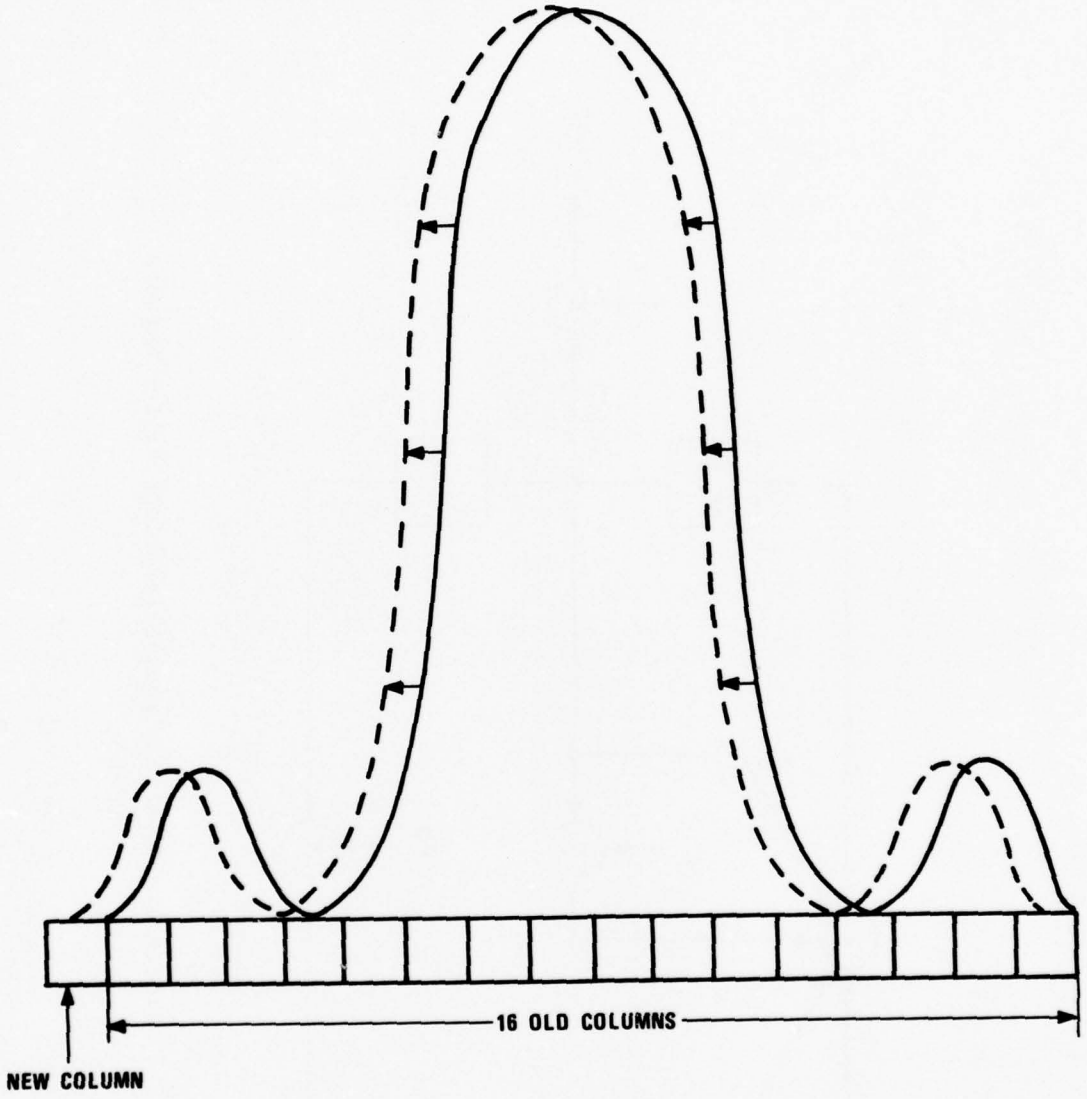


Figure 5. Antenna Weighting--Scan to the Left.

table is $2^{-10}$ circles (roughly the same as the 5-mil resolution of the AN/PPS-15's antenna read-out). The azimuth weight at each of these points is given by the formula

$$w(\theta_i) = \sqrt{\frac{1}{\Delta\theta} \int_{\theta_i - \frac{\Delta\theta}{2}}^{\theta_i + \frac{\Delta\theta}{2}} g^2(\phi)\, d\phi} \qquad (3\text{-}23)$$

where

$g(\phi)$ = one way power antenna gain normalized to one at the peak;

$\Delta\theta$ = clutter column width = 25 mils;

$\theta_i$ = azimuth position of a clutter column relative to the antenna beam position.

Notice that even though $g(\phi)$ is nonzero only over 16 clutter columns, the smearing effect of integrating over a clutter column width ($\Delta\theta$) for each value of $\theta_i$, causes the weights, $w(\theta_i)$, to have nonzero values over 17 clutter columns. The number of points in the table equals the angular width of 17 columns divided by the angular spacing in the table, i.e.,

$$\frac{(17)(1/256)}{2^{-10}} = 68 \quad .$$

The 68 weights are written into the random access memories from the EROS digital computer during simulation initialization (immediately preceding a simulation run).

To avoid spurious signals due to azimuth-weight discontinuities (refer to Section 2.7), the digital hardware linearly interpolates between points in the table*. This is, in fact, accomplished by interpolating both the azimuth readings and the table values in one operation. Recall that the azimuth samples are read at a rate 1/256 the Doppler sampling rate (refer to Section 2.9). For each of two successive azimuth readings, the corresponding arrays of 17 weights,

$$w_1, w_2, \ldots, w_{17}$$

and

$$w_1', w_2', \ldots, w_{17}' \quad ,$$

*Interpolation is feasible for clutter, because only the antenna moves. It would be much more difficult for targets, where both the antenna and the target may move.

are read from the clutter-azimuth weight table. An array weight increment

$$\Delta w_1, \Delta w_2, \ldots, \Delta w_{17}$$

is then computed such that

$$\Delta w_i = \frac{w_i' - w_i}{256} \quad .$$

The interpolated weights for the 17 clutter columns can thus be computed recursively for each Doppler cycle according to the formula

$$\left.\begin{aligned} w_i(0) &= w_i \\ w_i(k+1) &= w_i(k) + \Delta w_i \end{aligned}\right\} \quad \begin{aligned} &i = 1, \ldots, 17 \\ &k = 0, \ldots, 254 \end{aligned} \tag{3-24}$$

## 3.6 Pseudo Random Number Generator

The pseudo ramdom number generator was introduced briefly in Section 3.2, where it was observed that two points from which to select the random inputs are sufficient to attain the desired amplitude distribution. The spectral constraint on the random number generator was mentioned in the discussion of equation (3-9); that the autocorrelation function have 2 values, 1 value at 0-lag and a different value at non-0-lag. There is one additional constraint imposed by the finite register length of the filter implementation: that the magnitude $\gamma$ of the random input be sufficiently small to avoid filter overflow. This constraint can be expressed more precisely* in terms of the filter's unit-impulse response h(nT):

$$\hat{x} < \frac{1}{\sum_n |h(nT)|} \quad , \tag{3-25}$$

where $\hat{x}$ denotes the maximum magnitude of the total filter input. In addition to the pseudo-random input, $\hat{x}$ also includes the noise due to multiplier truncation. There are 2 multipliers in the filter; if $\hat{e}_1$ and $\hat{e}_2$ represent the maximum magnitudes assumed by their truncation errors, then (3-25) becomes

$$\gamma + \hat{e}_1 + \hat{e}_2 < \frac{1}{\sum_n |h(nT)|} \tag{3-26}$$

The denominator in (3-26) is large for low cut-off frequency filters, which restricts $\gamma$ in this case to small values (the smallest non-0 value for $\gamma$ consistent with the 16-bit number representation is $2^{-15}$). For higher cut-off

*c.f.[6], Section 9.3.2, pg. 427.

frequency filters the denominator in (3-26) decreases, and larger values of $\gamma$ can be used. Of course, it would be possible to use the same "safe" value of $\gamma$ ($2^{-15}$) for high and low frequency filters. But when the cut-off frequency is high, this would reduce the filter-output amplitude and restrict the dynamic range of the simulated radar cross-section. Therefore, the pseudo-random number generator has been implemented with a controllable magnitude which can be varied in powers of 2. The possible values of $\gamma$ range from $2^{-1}$ through $2^{-15}$.

The network describing the pseudo random number generator* is illustrated in Figure 6. It consists of 31 1-bit delay elements, an exclusive -OR gate, and decode logic to produce the possible outputs $+\gamma$ or $-\gamma$.

The generator has a cycle length of

$$p = 2^{31} - 1 \quad . \tag{3-27}$$

Two pseudo random inputs are required (one for each quadrature component) during every Doppler sampling cycle for each of the 544 clutter cells in the simulated antenna beam (refer to Section 3.5). The sampling period $T_1$ of the pseudo-random number generator is thus 1/1088 of the Doppler sampling period T. A portion of the pseudo-random sequence used on one of the 544 filters would not be reused on any of the other filters until 7.9 minutes later, and it would not be reused on the same filter until 2029 minutes later. Therefore, it is appropriate to treat the pseudo-random input as aperiodic. The relevant statistics of the pseudo-random number sequence $\rho(nT_1)$ are listed as follows:

The mean of $\rho(nT_1)$

$$\mu\{\rho\} = \gamma(2^{31} - 1)^{-1} = \gamma p^{-1} \quad . \tag{3-28}$$

The variance of $\rho(nT_1)$

$$\sigma^2\{\rho\} = \gamma^2 - \gamma^2 p^{-2} \quad . \tag{3-29}$$

The autocorrelation function of $\rho(nT_1)$

$$R_\rho(mT_1) = \begin{cases} \gamma^2 & m = 0 \\ -\gamma^2 p^{-1} & \text{otherwise} \end{cases} . \tag{3-30}$$

The random input to the complex filter (the pair of identical real filters) is denoted by r(nT). The relevant statistics of r(nT) are derived from (3-28), (3-29), and (3-30).

---

*The design and the statistical properties of the pseudo-random number generator were based on [7].

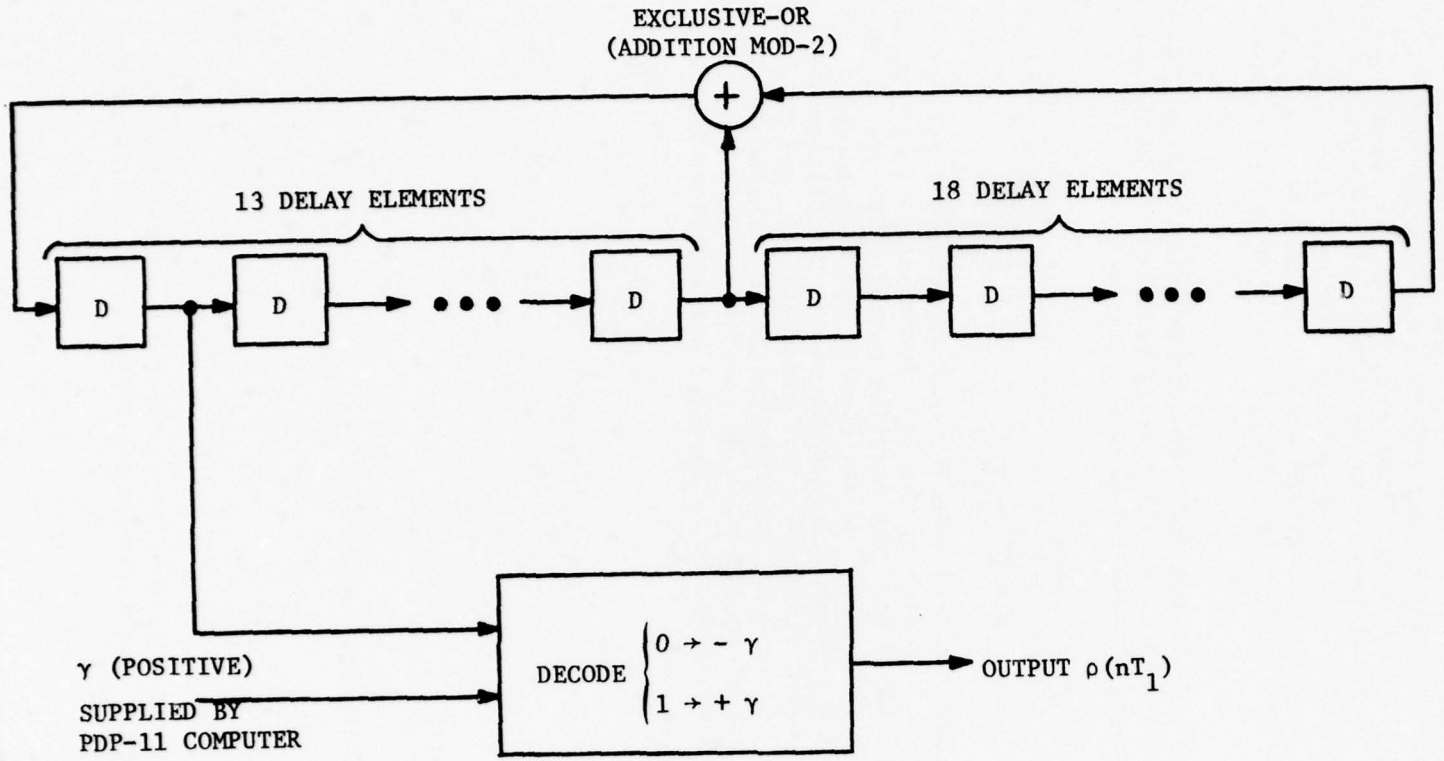


Figure 6. Pseudo-Random Number Generator.

The mean of r(nT)

$$\mu\{r\} = (1 + j)\gamma p^{-1} \quad . \tag{3-31}$$

The variance of r(nT)

$$\sigma^2\{r\} = 2(\gamma^2 - \gamma^2 p^{-2}) \quad . \tag{3-32}$$

The autocorrelation function of r(nT)

$$R_r(mT) = \begin{cases} 2\gamma^2 & m = 0 \\ -2\gamma^2 p^{-1} & \text{otherwise} \end{cases} \tag{3-33}$$

The mean and variance of r enter into the calculations of clutter radar cross section. The autocorrelation function (3-33) has the requisite spectral property--one value at 0-lag and a different value at non-0-lag.

The evaluation of $\gamma$ is based on the inequality (3-26). Expressions for $\hat{e}_1$ and $\hat{e}_2$ can be derived in terms of the feedback multipliers $\alpha_1$ and $\alpha_2$. The sum $\sum_n |h(nT)|$ is also a function of $\alpha_1$ and $\alpha_2$. However, a closed form expression has not been found for certain combinations of $\alpha_1$ and $\alpha_2$. Instead the sum is evaluated numerically using a software simulation of the filter. Section 2.3 of the Eighth EROS Quarterly Report contains a more detailed discussion of this calculation.

## 3.7 Clutter Filter Statistics

If the component of clutter due to non-moving scatterers is to have a specified radar cross-section $\sigma_1$, then it is necessary to calculate the constant term A in equation (3-5). This, in turn, requires that the mean $\mu$ of the filter output be known. Similarly, equation (3-6) indicates that in order to influence the radar cross-section $\sigma_2$ of the moving scatterers in clutter, it is necessary to be able to control the variance of the filter outputs. Since this is done by adjusting $\beta$, the post multiplier of the filter, an expression relating $\beta$ to the variance of the filter output is needed. The development in this section explains how these statistics are obtained.

The computations performed by the clutter digital filter of Figure 3 are described by the difference in equations for the states, $W_1$ and $W_2$, of the two delay elements. The independent variable, time, is expressed in multiples of the Doppler sampling period T (refer to Section 2.2).

$$W_1((n + 1)T) = \alpha_1 W_1(nT) + \alpha_2 W_2(nT) + x(nT) \tag{3-34}$$

$$W_2((n + 1)T) = W_1(nT) \tag{3-35}$$

$\alpha_1$ and $\alpha_2$ are the (real) feedback multiplier coefficients. The complex filter consists of two identical real filters. Therefore, it is correct to treat $W_1$, $W_2$ , and x as complex numbers. x(nT) is the sequence of random inputs, which includes both the pseudo-random numbers r(nT) and the contributions, $e_1(nT)$ and $e_2(nT)$, due to multiplier truncation errors,

$$x(nT) = r(nT) + e_1(nT) + e_2(nT). \tag{3-36}$$

The arithmetic performed by the digital filters employs 16-bit 2's complement binary fractions; the binary point is assumed to be between the sign bit and the 15 fraction bits. During each Doppler sampling cycle, the products $(\alpha_1 - 1)\ W_1$ and $\alpha_2\ W_2$ are formed, and the 30 fraction bits of each (real and imaginary) component of the product is truncated to 15 bits; the low-order 15 bits are discarded. If [a] denotes the largest integer that does not exceed a, and if [a + jb] denotes [a] + j[b], then the truncated products are expressed by $[2^{15}(\alpha_1 - 1)\ W_1]\ 2^{-15}$ and $[2^{15}\ \alpha_2\ W_2]\ 2^{-15}$. Therefore, the truncation errors are

$$e_1 = [2^{15}\ (\alpha_1 - 1)\ W_1]\ 2^{-15} - (\alpha_1 - 1)\ W_1 \tag{3-37}$$

and

$$e_2 = [2^{15}\ \alpha_2\ W_2]\ 2^{-15} - \alpha_2\ W_2 \quad . \tag{3-38}$$

The truncation error terms are derived from the low-order bits of product. In practice the two multipliers $\alpha_1 - 1$ and $\alpha_2$ are different. This implies that the cross covariance function of $e_1(nT)$ with $e_2(nT)$ is approximately 0. Moreover, the multiplicands $W_1(nT)$ and $W_2(nT)$ generally change values between cycles, which implies that the autocovariance functions of $e_1(nT)$ and $e_2(nT)$ are approximately 0. Similarly, the cross covariance functions of $e_1(nT)$ and $e_2(nT)$ with r(nT) are approximately zero. The relevant statistics of x(nT) follow from these statements and from equations (3-31), (3-32), (3-33), and (3-36).

The mean of x(nT)

$$\mu\{x\} = (1 + j)\ \gamma p^{-1} + \mu\{e_1\} + \mu\{e_2\} \quad . \tag{3-39}$$

The variance of x(nT)

$$\sigma^2\{x\} = 2(\gamma^2 - \gamma^2\ p^{-2}) + \sigma^2\{e_1\} + \sigma^2\{e_2\} \tag{3-40}$$

The autocorrelation function of x(nT)

$$R_x(mT) = \begin{cases} 2(\gamma^2 - \gamma^2 p^{-2}) + \sigma^2\{e_1\} + \sigma^2\{e_2\} & m = 0 \\ -2\gamma^2 p^{-1} - 2\gamma^2 p^{-2} + |\mu\{x\}|^2 & \text{otherwise.} \end{cases} \quad (3\text{-}41)$$

The expressions $\mu\{e_1\}$, $\mu\{e_2\}$, $\sigma^2\{e_1\}$, and $\sigma^2\{e_2\}$ represent the mean and variance of $e_1$ and $e_2$ respectively. Equations (3-39), (3-40), and (3-41) are used in the derivation of expressions for the mean and variance of $W_1$ and $W_2$. Moreover, equation (3-41) expresses the requisite spectral requirement for the filter input--that its autocorrelation function have one value at 0-lag and a different value at non-0-lag.

The mean and variance of $W_1$ and $W_2$ are now readily obtained. Note that $W_2$ is identical to $W_1$ except for a delay of one Doppler sampling cycle. Therefore, the statistics that describe $W_2$ are identical to those that describe $W_1$. Recall that $W_1$ can be represented as a convolution of the random process x with the unit-impulse response h(iT) of the filter.*

$$W_1(nT) = \sum_i h(iT)\, x(nT - iT) \quad (3\text{-}42)$$

The mean of $W_1$ follows immediately from (3-42)

$$\mu\{W_1\} = F(1 + j)\gamma p^{-1} + \mu\{e_1\} + \mu\{e_2\}), \quad (3\text{-}43)$$

where

$$F = \sum_i h(iT). \quad (3\text{-}44)$$

If $G^2$ denotes the sum of squares of the unit-impulse response

$$G^2 = \sum_i h^2(iT), \quad (3\text{-}45)$$

then a direct evaluation of the variance of $W_1$ yields

$$\sigma^2\{W_1\} = G^2\sigma^2\{x\} + R_x(\text{non-0})(F^2 - G^2) - F^2|\mu\{x\}|^2$$
$$= -2F^2\gamma^2(p^{-1} + p^{-2}) + G^2(2\gamma^2 + \sigma^2\{e_1\} + \sigma^2\{e_2\} + 2\gamma^2 p^{-1}) \; . \quad (3\text{-}46)$$

The computations of F and $G^2$ are simplified by the following formulas,

$$F = \frac{1}{1 - \alpha_1 - \alpha_2} \quad (3\text{-}47)$$

*Refer to Section 8.4 of [6].

and

$$G^2 = \frac{(1 - \alpha_2)}{(1 + \alpha_2)[(1 - \alpha_2)^2 - \alpha_1^2]} \quad . \tag{3-48}$$

Equations (3-43) and (3-46) express the mean and variance of $W_1$ as functions of the mean and variance of $e_1$ and $e_2$. Conversely, the mean and variance of $e_1$ and $e_2$ can be estimated from the mean and variance of $W_1$ by exploiting the fact that the quadrature components of $W_1$ are approximately Gaussian distributed. Therefore, an iterative algorithm can be employed to determine the mean and variance of $W_1$. The details of this algorithm are described in Section 2.4 of the Eighth EROS Quarterly Report. Included in the EROS software is a program to perform the iterations. Experience has shown that convergence generally occurs within at most three iterations.

The weighted filter output Y(nT) is related to $W_1(nT)$ by

$$Y(nT) = \beta W_1(nT) \quad . \tag{3-49}$$

Therefore, its mean and variance are expressed by

$$\mu\{Y\} = \beta\mu\{W_1\} \tag{3-50}$$

and

$$\sigma^2\{Y\} = \beta^2\sigma^2\{W_1\} \quad . \tag{3-51}$$

Combining (3-51) with (3-6) yields an expression for $\beta$ in terms of $\sigma_2$, the radar cross section of the moving clutter scatterers, and $\sigma^2\{W_1\}$, the variance of $W_1$.

$$\beta = \sqrt{\frac{\sigma_2}{K_\sigma \, \sigma^2\{W_1\}}} \tag{3-52}$$

(The constant $K_\sigma$ is defined in Section 2.8.)

The magnitude of the constant component of clutter backscatter is simply $\sqrt{\sigma_1/K_\sigma}$, where $\sigma_1$ denotes its radar cross section. Its phase $\phi$ is random (but constant), because the constant component represents the phasor sum of backscatter from many reflecting surfaces within the clutter cell, and each such phasor is randomly oriented. Thus, from equation (3-5) an expression for the additive constant can be derived.

$$A = \sqrt{\frac{\sigma_1}{K_\sigma}} \; e^{j\phi} - \beta\mu\{W_1\} \quad , \tag{3-53}$$

where $\phi$ is randomly selected from the uniform distribution on the interval $0 \leq \phi < 2\pi$.

# 4. TARGET SIMULATION

## 4.1 Target Data Management

The component of radar backscatter produced by targets is, as for clutter, represented by a complex envelope in digital form. The Doppler sampling frequency, 4.167 KHz, permits the unambiguous representation of radial velocities up to approximately 30 meters/second or 67 miles/hour.*

The samples of the target signal are obtained from analog recordings of coherently detected backscatter. Each sample consists of an in-phase and a quadrature component. For this purpose EROS contains two A/D converters, associated sampling and synchronization hardware, and software to store the samples on computer disk. For scaling purposes the user specifies the radar cross section of the recorded target.

In addition to sampled backscatter, target simulation also requires a description of maneuvers--the path on which the target moves and an association of points on the path with times during the simulation. The path is segmented into "legs"; the two endpoints of each leg are called "nodes". The target motion while traversing a leg is constant radial velocity and constant angular velocity. Legs form straight line segments on a B-scope display. For each leg the following information is provided:

- the (range, azimuth) coordinates of the nodes;
- the simulation times associated with the nodes;
- the name of a target recording or the specification that the target has disappeared during this leg;
- the portion of the recording to use;
- a weight (amplification or attenuation factor) to be applied to the radar cross section for the duration of the leg.

The weight can be used to account for partial masking.

A computer program called "target compilation" combines this data and stores it on disk in a form that is optimal for real-time retrieval. For each Doppler sampling cycle the target's azimuth and range are computed. Seventeen-bit azimuth accuracy is retained in accordance with Section 2.7. The instantaneous range of the target is expressed in terms of range-ring numbers; the user will have specified the range from the radar to the closest simulated

*This is based on the AN/PPS-15 radar's transmitter frequency of 10.2 to 10.4 GHz.

ring, and the rings are 15.027 meters wide (see Section 2.1). The apportionment of the target sample between two adjacent range rings has been described in Section 1.2. Each Doppler sampling cycle is represented by four 12-bit sample components: the portions of the in-phase and quadrature components in range-ring r and in range-ring r + 1. These samples are stored in four 16-bit words. The remaining 16 bits not occupied by the sample components contain range-ring data, azimuth data, and synchronization information.

During real-time simulation the computer retrieves the target data, compares its azimuth with that of the antenna beam, obtains an azimuth weight from an antenna-pattern table, and transmits information to the digital hardware:

- the antenna pattern weight;
- the in-phase and quadrature components;
- the range-ring number;
- synchronization information.

The digital hardware multiplies the sample components by the weight and combines the products with the clutter samples at the appropriate range rings.

## 4.2 Real-Time Limitations

The time interval of 240 μsec between target samples imposes a significant burden on the computer during real-time simulation. Much of the effort in preparing a target sample is expended in interacting with the subject radar's antenna. It would be impossible for the computer to perform the antenna-pattern multiplications in real-time. For this reason the target azimuth weighting is done in the special purpose digital hardware.

Even without having to perform the multiplications, a substantial amount of time is required in each Doppler sampling cycle to look up the azimuth weight and to transmit the data to the digital hardware. Timing measurements indicate that more than 100 μsec are needed to perform the computation for one target during each 240 μsec Doppler cycle. Since the computer has to provide clutter parameters in addition to the target samples, the computer would not be capable of simulating more than one target in the antenna beam at a time.

The following restrictions have been imposed on the target portion of the scenario to meet the real-time requirements:

- A target scenario can consist of one or two target paths. The target paths consist in general of several legs. Associated with each target path are sectors defined by a beginning azimuth and an ending azimuth. All nodes of the path must fall between these two azimuths.

- Each target path can contain several targets, but only one target at a time. The legs are simulated in sequence.

- The angle between the beginning and ending azimuth must be 2734 mils or less.

- The sectors of the two paths must not overlap. The sectors must be separated by at least 500 mils.

## 4.3 Target Sample Blocking

Consider the schedule for target processing shown in Figure 7(a). Real-time processing is subdivided into 240 μsec intervals. The target data for each Doppler sampling cycle are sent to the digital hardware at the beginning of each of these intervals. The remaining time at the end of the 240 μsec interval is available for supplying clutter parameters. In order to alert the computer to start target processing at the beginning of each interval, either interrupts must be provided at a 4.167 KHz frequency, or the clutter program must check a status flag frequently. The interrupt method is unsatisfactory, because the time required to switch status (including saving and restoring contents of six general-purpose registers) would severely aggravate the real-time load. The frequent checking of the status flag within the short time available at the end of the 240 μsec interval is similarly infeasible.

An alternative schedule which resolves these difficulties is shown in Figure 7(b). Real-time processing is subdivided into intervals of length 240 n μsec, where n equals 128 for the current version of EROS. The target data for n Doppler sampling cycles are sent to the digital hardware at the beginning of each of these intervals. The remaining time at the end of each interval is now in a more usable form for performing clutter processing. The digital hardware alerts the computer at the end of each 240 n μsec interval by setting a status bit.

Buffer storage must be provided to hold a block of data since it is generated well in advance of the time the radar would receive that target signal. The storage could have been part of the computer's core memory instead of dedicated random-access memory in the digital hardware. The latter choice was made for a number of reasons, including software simplicity, elimination of need for direct-memory-access hardware, and reduction of the computer's core-memory usage. Two such buffers are provided, so that the computer can be writing into one of them while the hardware reads previously stored data from the other one.

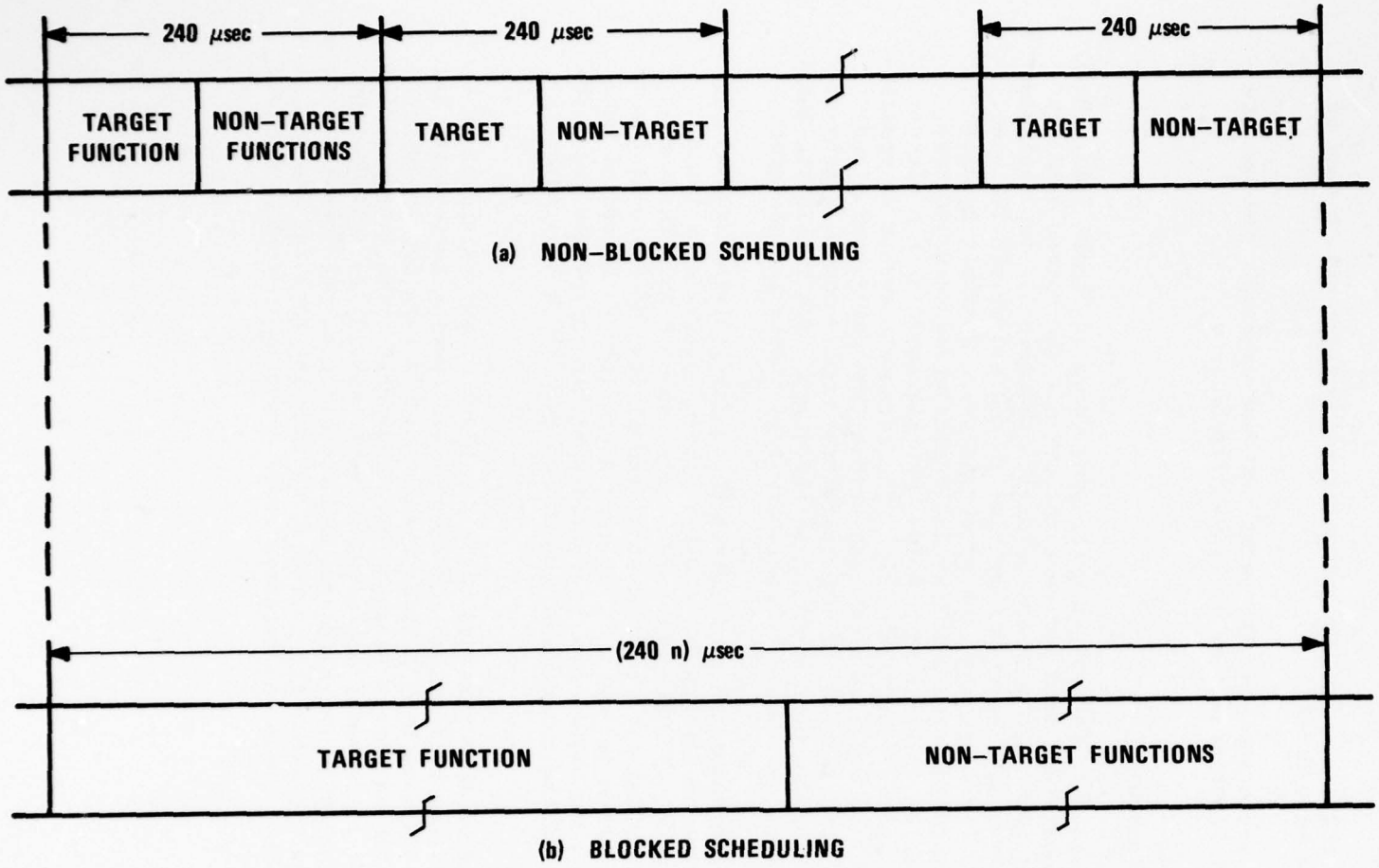


Figure 7. Scheduling of Real-Time Computer Functions.

# 5. EROS IMPLEMENTATION

This section presents brief descriptions of the major units comprising the EROS implementation.

## 5.1 Simulation Preparation Software

Simulation preparation software consists of programs to assist the operator in describing the scenario. Much of the information is maintained in reference files (called "libraries"), whose contents may have widespread applicability in many scenarios. All input entered by the user is checked for validity, and diagnostics are written when errors are detected. Generous provision is made for the user to append comments to document his simulation data. Optional printouts permit the user to generate reference reports that define the files' contents and that contain the user-written comments.

The records in the clutter spectral library specify the spectral properties of the clutter filters. Each record corresponds to a different spectral behavior, and is identified by a unique integer. Facilities are provided for the EROS user to add or change records in this library.

The complete clutter library consists of records which contain both spectral and radar cross section information. To define a record in this library, the user supplies (1) a 2-character code to identify the record; (2) an integer that refers to a record in the clutter spectral library; and, (3) radar cross section values for the fixed and moving components of clutter. The clutter library update program retrieves the spectral information inferred by the given spectral-reference integer. Facilities are provided for the EROS user to add, delete, or change records in the library.

The clutter scenario description program assists the user in defining the positional dependence of clutter. The computer's graphic cathode-ray-tube and light pen are made available to the user to expedite his definition of the 8192-cell clutter description array. The type of clutter in each cell is identified by the two-character code that refers to a record in the complete clutter library. The user may also need to define a clutter weight array, which specifies an amplification or attenuation to be applied to the radar cross section in each cell. The weights can account for partial masking, range dependence of the cell's areas, incidence angle effects, etc. A unique file name is associated with each clutter description array and each clutter weight array. Facilities are provided for the EROS user to revise an array or to define a new array as a modification to a previously defined array. The clutter scenario compilation program combines specified arrays and reference-file information to produce the "compiled clutter scenario file" in an optimal format for real-time simulation.

The target portion of a scenario is built up from recordings and from target path definitions. The recorded information extracted from the A/D converters is stored on disk files as described in Section 4.1. A unique file name is associated with each recording. The computer's cathode-ray-tube and light pen are available to the user for describing the target paths, which are depicted in the form of a B-scope display. The target compilation program combines one or two target paths and the recordings referenced in these paths. It produces the "compiled target scenario file" in an optimal format for real-time simulation.

Antenna patterns are represented during real-time simulation by a 4096-point table for attenuating target signals and by a 68-point table for attenuating clutter signals. The user specifies the pattern with 13 points spaced at 1-degree intervals from the beam center. The computer translates this specification into an antenna pattern file which holds the two tables; formula (3-23) is used to calculate the clutter antenna pattern table.

The range-weight file consists of 197 attenuation factors corresponding to range rings from 60 to 3000 meters at 15-meter intervals. Specified range-weight inputs are converted to fixed-point format for real-time simulation. Note that only 64 of these weights are used during any given simulation run. The minimum range for the simulation determines which of these 64 weights to use.

## 5.2 Real-Time Software

The user initiates a simulation run by entering the name of an "EROS scenario file". EROS scenario files, which are created by the user via the operating system's text editor, contain the names of the component files:

- a compiled clutter scenario file,
- a compiled target scenario file,
- an antenna pattern file,
- a range-weight file.

During simulation initialization, various tables and constants are read into the computer and into digital-hardware memories. These include the antenna-pattern and range-weight tables. EROS starts producing simulated backscatter when the radar's antenna reaches a specified azimuth and is proceeding in a specified scan direction. This increases the repeatability of EROS experiments. After simulation has started, the real-time program responds to the antenna's azimuth by copying appropriate clutter and target data from the disk files to the digital hardware.

## 5.3 Digital Hardware

The digital hardware performs those functions, where the speed and the number of computations are beyond the real-time capability of the computer. The data inputs to the digital hardware are supplied by the computer:

- filter parameters and current azimuth for clutter;
- signal samples, range, and azimuth weight for targets.

The clutter processor continuously calculates synthetic clutter backscatter from the 544 cells in the currently simulated antenna beam. Each Doppler sampling cycle consists of performing one computation step for each filter, applying the antenna pattern weights, and performing azimuth integration. The azimuth input from the computer is used to determine which antenna-pattern weight applies to a given cell. Azimuth integration consists of adding together the returns from cells at the same range. The result is a sampled profile of clutter return

$$s_0, s_1 \cdots s_{63}$$

spaced at 15-meter intervals, such that

$$s_0 = s_1$$

$$s_2 = s_3$$

$$\cdots$$

$$s_{62} = s_{63} \quad .$$

The values of these 64 samples are recalculated each 240 μsec.

The target processor applies the azimuth weight to the two quadrature components of each target sample and stores the products with the associated range-ring number in a random access memory (RAM). In general, two such sets of data are required for each Doppler sampling cycle, because part of a target sample is allocated to one range ring, and the balance is allocated to an adjacent range ring. The RAM is capable of storing data for 128 Doppler sampling cycles. Status bits are stored in the RAM to denote the end of each Doppler sampling cycle and the end of 128 Doppler sampling cycles. Two such RAM's are used, so that the computer can load one of them while the target processor retrieves previously loaded data from the other one. Each retrieved sample is added to the clutter range profile at the range specified by the retrieved range-ring number.

The video signal is produced by storing each range profile in a RAM and by reading it back at the radar's pulse repetition frequency (PRF). Since the Doppler sampling frequency is 1/9 the PRF of the AN/PPS-15 radar (see

Section 2.2), each range profile is read back nine times. Two RAM's are used for this purpose, so that one of them can be loaded from the target processor while the video signal is read from the other one.

Four clocks are used to synchronize the digital hardware. The clutter and target processors employ a 10 MHz clock derived from a crystal oscillator and a 4.167 KHz clock derived by dividing the radar's 37.5 KHz PRF by 9. The video signal generator employs the 4.167 KHz clock for loading the RAM's; for reading back the video signal it employs the 37.5 KHz PRF clock and a 10 MHz clock derived from a quenched oscillator. The 10 MHz frequency corresponds to the 15-meter range-ring spacing. The quenched oscillator is restarted by a signal derived from the radar's PRF trigger and provides a stable representation of the delay between radar transmission and reception.

## 5.4 Analog Hardware

Analog hardware is needed in any radar signal simulation to convert digital samples into a form suitable for insertion into the radar. Moreover, in EROS the range-weighting and range-integration functions are performed in analog hardware to meet the AN/PPS-15 radar's dynamic-range and video-bandwidth capabilities. A preliminary design*, in which these computations were to be performed digitally, was rejected in order to improve signal quality and to simplify hardware and software.

Twelve-bit D/A converters are available with speeds adequate to process real-time video signals. Three such converters are used: (1) to convert sign and magnitude of In-phase (I) data prior to range weighting; (2) to convert sign and magnitude of Quadrature (Q) data prior to range weighting; and (3) to convert magnitude of the range weight values. The analog output of the range weight D/A converter is multiplied by the I signal and by the Q signal in separate analog multipliers.

For video signal simulation, digital signals representing the I and Q content and range weight of successive range rings are latched into the three D/A converters at 100 nanosecond intervals. Outputs of the analog multipliers are integrated in analog integrators, which are reset periodically by pulses coincident with the transmitter modulation. Since signals from all range rings are present for equal time increments, integration with respect to time is equivalent to algebraic addition of the data from successive range rings. The output from the integrators is a faithful representation of the envelope of AN/PPS-15 radar return, because the radar transmits CW with 180° phase reversals at the PRF. The integrators are also quite effective in reducing the bit-switching transients that are inherent in D/A converters. The output of the integrators are fed into variable-gain video amplifiers, which provide calibration and the addition of adjustable simulated receiver noise. Simple band-pass filters are used to limit the video signal bandwidth to that of the radar pre-amplifier, and to further attenuate bit-switching transients that originate in the D/A converters.

---

*Refer to Section 4 of the Fourth EROS Quarterly Report.

For simulation of range-gated Doppler signals, the EROS operator selects one of the 64 range rings by means of a knob on the analog hardware. Digital signals representing the I content, Q content, and range weight of the selected range ring are latched into the D/A converters at the transmitter modulation rate, and each sample is held for a time equal to the interval between transmitter modulations. The range integrators have been switched out, and the range weighting analog multipliers are connected through low-pass filters to variable-gain Doppler output amplifiers.

The present method of analog range weighting lends itself readily to simulation of other types of radar modulation. In particular, the bipolar video signal of conventional pulse-Doppler radar differs from the AN/PPS-15 video in that the returns from a single range resolution cell contribute to the video signal at any given point in the interpulse interval. This signal is simulated in EROS simply by switching out the range integrator and adjusting signal and noise levels appropriately for the parameters of the radar under test. The range-gated Doppler signal for pulse modulation and for the AN/PPS-15 modulation do not differ in form, and only the adjustment of signal and noise levels is required.

## 5.5 Current Status

Each of the component units of EROS has been fabricated and unit tested. The software has been written, debugged, and system tested. However, the integration of these components is still in progress and a complete system test will be conducted under the Contract DAAB07-77-C-2174, which is an extension of the current program.

# APPENDIX

## EFFECT OF DISCRETE REPRESENTATION OF ANTENNA PATTERN

The effect of the antenna pattern in the horizontal plane is simulated in EROS by applying an appropriate weight to the radar return from each backscatter element. The weight depends upon the difference between the azimuth angle describing the location of the backscatter element and the azimuth angle of the antenna direction. The value of the weight equals the two-way voltage antenna gain function evaluated at this angle difference. A tabular representation of the antenna gain function will be used in EROS for two reasons:

(1) the computer can perform table lookups faster than calculate a formula;

(2) greater flexibility is permitted in representing the antenna pattern; e.g., measured antenna gain data can be applied to the simulation even if the data cannot be conveniently reduced to a formula.

A small number of table entries (e.g., less than 50) would be adequate for accurate representation of antenna gain if linear interpolation were used. However, the computation time required to perform even linear interpolation would add a significant burden to the computer's real-time load. To avoid interpolation, we would design the antenna pattern table with a large number of values of the gain function at evenly spaced angles. The real-time target-processing program would then select the table value whose corresponding angle is closest to the target's azimuth difference.

Consider the effect of scanning at constant angular rate across a stationary reflector with large radar cross section (e.g., a corner reflector). The radar return signal is amplitude modulated by the antenna gain function, while the angle is varied at the antenna scan rate. Let $\alpha$ denote the angular rate of antenna scan, and $\Delta\theta$ denote the angular separation between adjacent points in the antenna gain function table. Using this tabular representation of antenna gain, an EROS simulation of the corner reflector scenario would produce the staircase function shown in Figure 8. The simulated signal remains constant for a duration of $\frac{\Delta\theta}{\alpha}$ and then jumps to the next value in the table. Of course, if $\frac{\Delta\theta}{\alpha}$ is less than the 240 μsec sampling interval, the simulation is perfectly adequate. However, for larger values of $\Delta\theta$ the jump discontinuities increase in magnitude and decrease in frequency, and they introduce spurious signals at frequencies within the pass band of the AN/PPS-15. It is therefore of interest to determine the largest tolerable value of $\Delta\theta$ for which the spurious signal is at a sufficiently low power. The following analysis addresses this question.

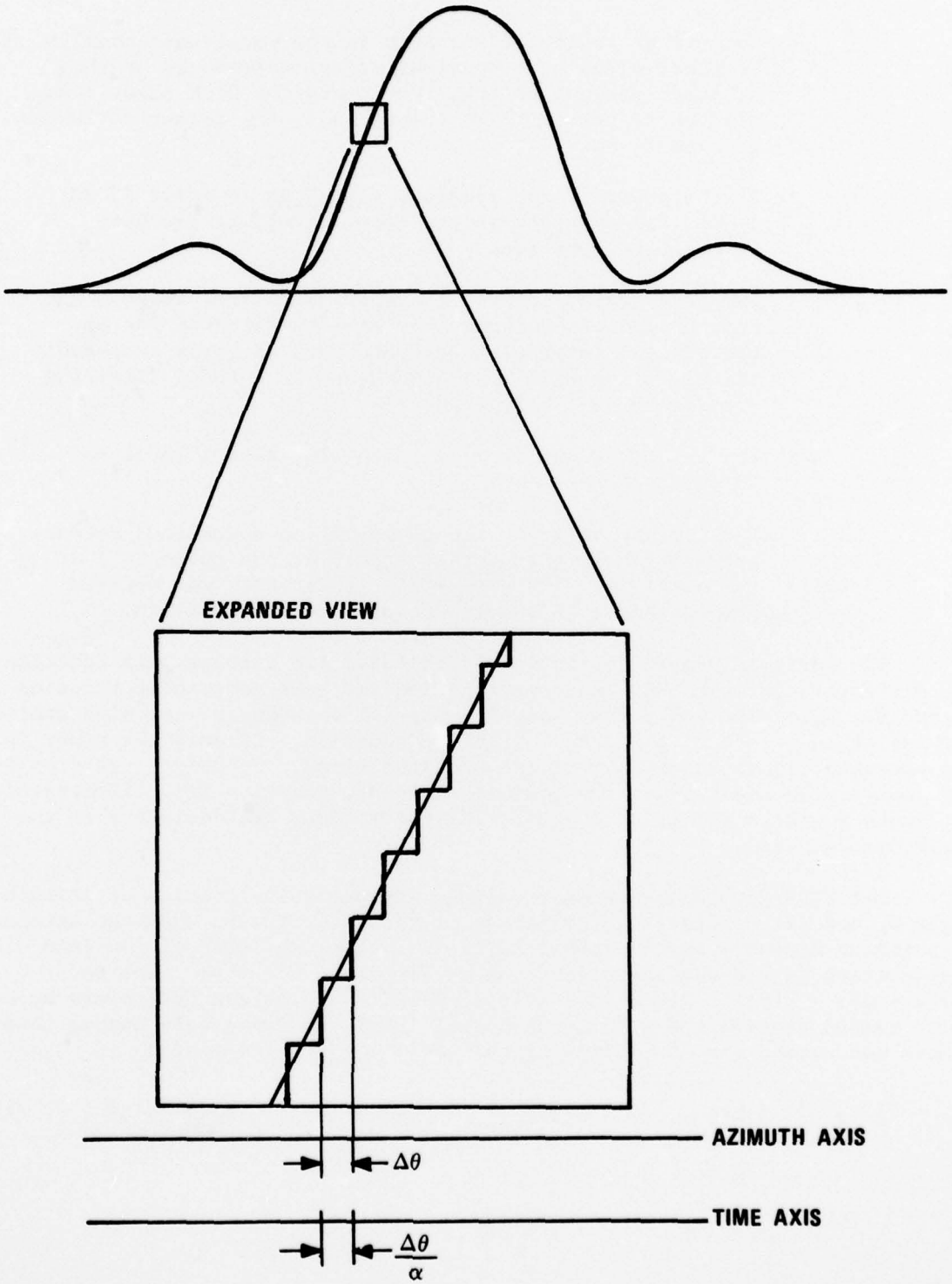


Figure 8. Simulation of Antenna Scan Modulation with Discrete Representation of Antenna Gain.

In performing this analysis several assumptions were made:

- The corner reflector scenario is the worst-case problem. In other words, the spurious signal introduced by the discrete antenna pattern representation with other illuminated targets will be tolerable if the corner reflector problem is solved.

- If the power of the spurious signal is at least 72 dB lower than the saturating signal level, it has been adequately suppressed.

- Frequency components of the spurious signal above 3 kHz can be ignored, because they will be filtered out by the digital interpolation up to 37.5 kHz, the post-audio filter in the EROS analog hardware, and audio filtering within the AN/PPS-15 radar.

- The antenna scans at a fixed angular rate $\alpha$ equal to 90 mils/second.

- The largest value of the slope of the normalized antenna pattern (whose gain varies from 0 at the nulls to 1 at the nose) is .0138 $\frac{\text{unit gain}}{\text{mil}}$. This value was derived from a sample AN/PPS-15 measured antenna pattern.

The spurious signal introduced by the discrete antenna gain function is the difference between the staircase function and scan modulation function in Figure 8. This spurious signal has the shape of a sawtooth wave with amplitude varying as the slope of the scan modulation function. Clearly the power in the sawtooth signal is maximum at the steepest slope. Therefore, we simplify the analysis by considering the periodic sawtooth function E(t) illustrated in Figure 9. whose amplitude a equals 1/2 the maximum discontinuity in the staircase function.

Let $W(\theta)$ denote the two-way voltage antenna gain function of azimuth angle $\theta$, and let A denote the amplitude of the radar return when the antenna is pointing directly at the corner reflector. The magnitude of the jump discontinuities in the staircase function of Figure 8. are thus equal to $A|W(\theta + \Delta\theta) - W(\theta)|$. Since EROS scenarios will not include reflectors whose radar return exceeds the saturating signal level, we can safely assume that A does not exceed the saturating signal level $A_{max}$. Therefore,

$$a = \frac{1}{2} A|W(\theta + \Delta\theta) - W(\theta)|_{max} = \frac{1}{2} A \lambda \Delta\theta \leq \frac{1}{2} A_{max} \lambda \Delta\theta . \qquad (A1)$$

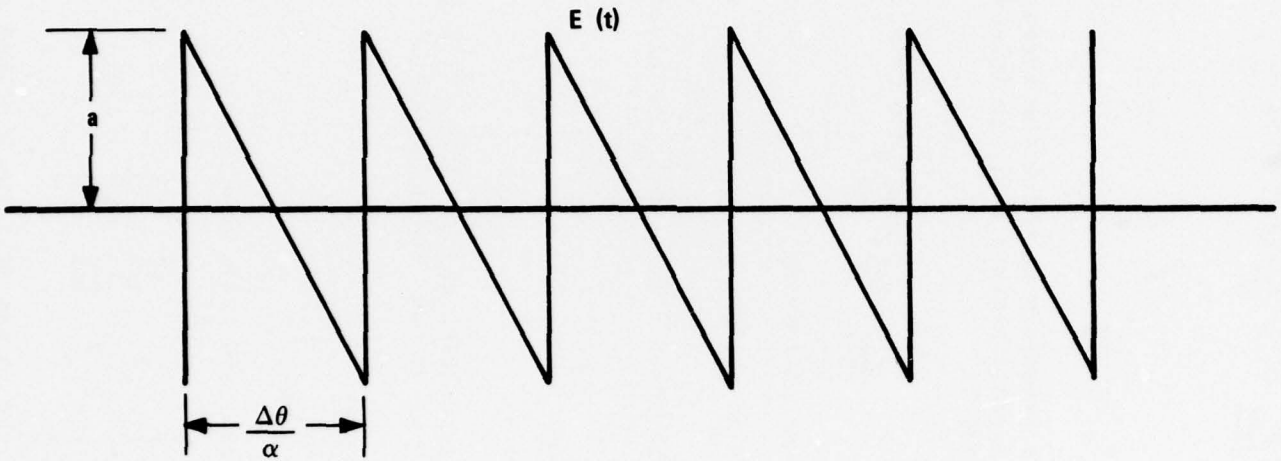


Figure 9. Sawtooth Error Function Due to Discrete Representation of Antenna Scan Modulation.

The Fourier series representation of E(t) is

$$E(t) = \sum_{n=-\infty}^{\infty} (-1)^n \frac{aj}{n\pi} e^{j\, n\, 2\pi\, f_o\, t} \quad ,$$

where

$$f_o = \frac{\alpha}{\Delta\theta} \quad . \tag{A2}$$

Note that $f_o$ denotes the frequency at which the antenna gain function is sampled. After filtering out components above 3 kHz, the low-pass filtered error function $[E(t)]_{LP}$ is expressed by

$$[E(t)]_{LP} = \sum_{n=-k}^{k} (-1)^n \frac{aj}{n\pi} e^{j\, n\, 2\pi\, f_o\, t} \quad ,$$

where k is largest integer satisfying

$$f_o k < 3000 \quad . \tag{A3}$$

By Parseval's theorem the power P in $[E(t)]_{LP}$ is given by

$$P = \sum_{\substack{n=-k \\ n\neq 0}}^{k} \left(\frac{a}{n\pi}\right)^2 \quad . \tag{A4}$$

Since the power in the saturating signal is $A_{max}^2$, and since P must be at least 72 dB below the power of the saturating signal,

$$10 \log_{10} \left[\frac{P}{A_{max}^2}\right] \leq -72 \quad . \tag{A5}$$

Combining (A1), (A2), (A4), and (A5), we get

$$10 \log_{10} \left[\frac{\lambda^2 \alpha^2}{2\pi^2 f_o^2} \sum_{n=1}^{k} \frac{1}{n^2}\right] \leq -72 \quad . \tag{A6}$$

Finally by substituting the values of $\lambda$ and $\alpha$ stated in the assumptions, we compute the smallest $f_o$ satisfying (A3) and (A6) to be 1244 Hz. By (A2) the corresponding angular-resolution constraint is that $\Delta\theta < .0723$ mils = $1.13 \times 10^{-5}$ circles. Since angles will be expressed during EROS simulation in terms of binary fractions of a circle, at least 17 bits are required to attain this angular resolution.

## REFERENCES


1. Davenport, Wilbur E., and Root, William L., An Introduction to the Theory of Random Signals and Noise, McGraw-Hill, 1958.

2. Wood, W. E., Pope, B. E., and Dunlop, S. O., Digital Simulation of Radar Clutter, Report No. RE-TM-72-1, U.S. Army Missile Command, Redstone Arsenal, Alabama, August 1972.

3. Goldstein, H., "The Fluctuations of Clutter Echoes," Propagation of Short Radio Waves, Vol. 13, D. E. Kerr (Editor), M.I.T. Radiation Laboratory Series, 1951, pp. 550-587.

4. Fischbein, W., Graveline, S. W., and Rittenbach, O. E., "Clutter Attenuation Analysis," Technical Report ECOM 2808, March 1967.

5. Currie, N. C. , Dyer, F. B., and Hayes, R. D., "Radar Land Clutter Measurements at Frequencies of 9.5, 16, 35, and 95 GHz," Technical Report No. 3, Project A-1485, Georgia Institute of Technology, Engineering Experiment Station, April 1975.

6. Oppenheim, Alan V., and Schafer, Ronald W., Digital Signal Processing, Prentice Hall, Englewood Cliffs, N.J., 1975.

7. Golomb, Solomon W., Shift Register Sequences, Holden-Day, Cambridge, Massachusetts, 1967.

HEADQUARTERS
US ARMY ELECTRONICS COMMAND
FORT MONMOUTH, NJ 07703

AMSEL-CT-R

TITLE OF REPORT: Environment and Radar Operation Simulator (EROS)
CONTRACT NUMBER: DAAB-74-C-0272
CONTRACTOR: Georgia Institute of Technology

DISTRIBUTION LIST

| | NR. OF COPIES |
|---|---|
| Defense Documentation Center<br>ATTN: DDC-TCA<br>Cameron Station (Bldg 5)<br>Alexandria, VA 22314 | 1 |
| Defense Intelligence Agency<br>ATTN: DIADT-3C<br>Washington, DC 20301 | 1 |
| Dir, National Security Agency<br>ATTN: TDL<br>Ft George G. Meade, MD 20755 | 1 |
| Dir, Defense Nuclear Agency<br>ATTN: Technical Library<br>Washington, DC 20305 | 1 |
| Naval Ship Engineering Center<br>ATTN: Code 6179B<br>Prince Georges Center Bldg<br>Hyattsville, MD 20782 | 1 |
| Cdr, Naval Electronics Lab Center<br>ATTN: Library<br>San Diego, CA 92152 | 1 |
| Cdr, US Naval Ordnance Lab<br>ATTN: Technical Library<br>White Oak, Silver Spring, MD 20910 | 1 |
| Commandant, Marine Corps<br>HQ US Marine Corps<br>ATTN: Code A04C<br>Washington, DC 20380 | 1 |

AMSEL-CT-R
Distribution List for Contract DAAB07-74-C-0272, Georgia Inst of Technology

| | NR. OF COPIES |
|---|---|
| Communications-Electronics Division<br>Development Center<br>Marine Corps Dev & Educ Command<br>Quantico, VA 22134 | 1 |
| Cdr, US Naval Weapons Lab<br>ATTN: KEB-2F(FENN)<br>Dahlgren, VA 22448 | 1 |
| Rome Air Development Center<br>ATTN: Documents Library (TDLD)<br>Griffiss AFB, NY 13440 | 1 |
| HQ ESD (TRI)<br>L. G. Hanscom Field<br>Bedford, MA 01730 | 1 |
| Air Force Avionics Laboratory<br>ATTN: AFAL/DOT (STINFO)<br>Wright-Patterson AFB, OH 45433 | 1 |
| Armament Development & Test Center<br>ATTN: SSLT<br>Eglin AFB, FL 32542 | 1 |
| HQ, Air Force Systems Command<br>ATTN: DLTE<br>Andrews AFB<br>Washington, DC 20331 | 1 |
| Air Force Weapons Laboratory<br>ATTN: Technical Library (SUL)<br>Kirtland AFB, NM 87117 | 1 |
| Cdr, US Army Training & Doctrine Cmd<br>ATTN: ATTS-X<br>Fort Monroe, VA 23651 | 1 |
| HQDA (DAFD-CN)<br>Washington, DC 20310 | 1 |
| HQDA (DACE-ED)<br>Washington, DC 20314 | 1 |

AMSEL-CT-R
Distribution List for Contract DAAB07-74-C-0272, Georgia Inst of Technology

| | NR. OF COPIES |
|---|---|
| Ofc, Asst Secy of the Army (R&D)<br>ATTN: Assistant for Research<br>Rm 3-E-379, The Pentagon<br>Washington, DC 20310 | 1 |
| Cdr, US Army Training & Doctrine Cmd<br>ATTN: ATCD-SI<br>Fort Monroe, VA 23651 | 1 |
| HQDA (DARD-ARP/Dr. R. B. Watson)<br>Washington, DC 20310 | 1 |
| Cdr, US Army Materiel Command<br>ATTN: AMCRD-O<br>5001 Eisenhower Ave<br>Alexandria, VA 22333 | 1 |
| Cdr, US Army R&D Group<br>(Far East)<br>APO, San Francisco, CA 96343 | 1 |
| Cdr, USA Missile Command<br>Redstone Scientific Info Center<br>ATTN: Ch, Document Section<br>Redstone Arsenal, AL 35809 | 1 |
| Cdr, US Army Training & Doctrine Cmd<br>ATTN: ATCE<br>Fort Monroe, VA 23651 | 1 |
| Cdr, USA Weapons Command<br>ATTN: AMSWE-REF<br>Rock Island, IL 61201 | 1 |
| Cdr, US Army Combined Arms Combat Dev Activity<br>ATTN: ATCAIC<br>Fort Leavenworth, KS 66027 | 1 |
| HQ, USA Aviation Systems Command<br>ATTN: AMSAV-C-AD<br>P. O. Box 209<br>St. Louis, MO 63166 | 1 |

AMSEL-CT-R
Distribution List for Contract DAAB07-74-C-0272, Georgia Inst of Technology

| | NR. OF COPIES |
|---|---|
| Cdr, Harry Diamond Laboratories<br>ATTN: Library<br>Washington, DC 20438 | 1 |
| Cdr, USA Foreign Sci & Tech Cen<br>ATTN: AMXST-IS1<br>220 Seventh St., NE<br>Charlottesville, VA 22901 | 1 |
| Cdr, USA Picatinny Arsenal<br>ATTN: SMUPA-VC5 (Mr. P. Kisatsky)<br>Bldg 350<br>Dover, NJ 07801 | 1 |
| Cdr, Frankford Arsenal<br>ATTN: Library, H1300, Bldg 51-2<br>Philadelphia, PA 19137 | 1 |
| Cdr, White Sands Missile Range<br>ATTN: STEWS-RE-10 (Mr. G. Galos)<br>White Sands Missile Range, NM 88002 | 1 |
| Dir, USA Ballistic Research Lab<br>ATTN: AMXBR-VL (Mr. D. L. Riggotti)<br>Aberdeen Proving Ground, MD 21005 | 1 |
| Cdr, USA Mat & Mech Rsch Center<br>ATTN: AMXMR-ATL (Tech Library Br)<br>Watertown, MA 02172 | 1 |
| President, USA Artillery Board<br>Fort Sill, OK 73503 | 1 |
| Cdr, Aberdeen Proving Ground<br>ATTN: Technical Library, Bldg 313<br>Aberdeen Proving Ground, MD 21005 | 1 |
| Cdr, USA Electronic Proving Ground<br>ATTN: STEEP-MT<br>Fort Huachuca, AZ 85613 | 1 |
| Cdr, USASA Test & Evaluation Center<br>Fort Huachuca, AZ 85613 | 1 |

AMSEL-CT-R
Distribution List for Contract DAAB07-74-C-0272, Georgia Inst of Technology

| | NR. OF COPIES |
|---|---|
| USA Research Office - Durham<br>ATTN: Dr. Robert J. Lontz<br>Box CM, Duke Station<br>Durham, NC 27706 | 1 |
| Cdr, USA Mobility Eqpt R&D Center<br>ATTN: Tech Docu Cntr, Bldg 315<br>Fort Belvoir, VA 22060 | |
| USA Security Agency<br>ATTN: IARD<br>Arlington Hall Sta, Bldg 420<br>Arlington, VA 22212 | 1 |
| Cdr, USA Tank-Automotive Command<br>ATTN: AMSTA-RH-FL<br>Warren, MI 48090 | 1 |
| Technical Support Directorate<br>ATTN: Technical Library, Bldg 3330<br>Edgewood Arsenal, MD 21010 | 1 |
| Cdr, US Army Combined Arms Combat Dev Activity<br>ATTN: ATCACC<br>Fort Leavenworth, KS 66027 | 1 |
| Cdr, USA Dugway Proving Ground Library<br>ATTN: STEDP-TL (Tech Library)<br>Dugway, UT 84022 | 1 |
| Cdr, Yuma Proving Ground<br>ATTN: STEYP-AD (Tech Library)<br>Yuma, AZ 85364 | 1 |
| Cdr, US Army Materiel Command<br>ATTN: AMCRD-R<br>5001 Eisenhower Avenue<br>Alexandria, VA 22333 | 1 |
| Commandant, US Army Infantry Sch<br>ATTN: ATSIN-CTD<br>Fort Benning, GA 31905 | 1 |

AMSEL-CT-R
Distribution List for Contract DAAB07-74-C-0272, Georgia Inst of Technology

| | NR. OF COPIES |
|---|---|
| Commandant, USA Field Artillery School<br>ATTN: Target Acquisition Dept<br>Fort Sill, OK 73503 | 1 |
| Cdr, USA Systems Analysis Agency<br>ATTN: AMSRD-AMB (Mr. A. Reid)<br>Aberdeen Proving Ground, MD 21005 | 1 |
| Cdr, USA Tank-Automotive Cmd<br>ATTN: AMSTA-Z (Dr. J. Parks)<br>Warren, MI 48090 | 1 |
| Ch, Missile EW Technical Area<br>EW Laboratory (ECOM)<br>White Sands Missile Range, NM 88002 | 1 |
| Ch, Intelligence Mat Dev Ofc<br>EW Laboratory (ECOM)<br>Fort Holabird, MD 21219 | 1 |
| NASA Sci & Tech Info Facility<br>ATTN: Acquisitions Br (S-AK/DL)<br>P. O. Box 33<br>College Park, MD 20740 | 1 |
| Target Signature Analysis Center<br>Willow Run Labs - Inst of Science & Technology<br>University of Michigan<br>P. O. Box 618<br>Ann Arbor, MI 48107 | 1 |
| Remote Area Conflict Info Center<br>Battelle Memorial Institute<br>505 King Avenue<br>Columbus, OH 43201 | 1 |
| Martin Marietta Corporation<br>ATTN: MS 0452 (Lynes)<br>P. O. Box 179<br>Denver, CO 80201 | 1 |
| Cdr, Rome Air Development Center<br>ATTN: Mr. John C. Cleary/OCSA<br>Griffiss AFB, NY 13441 | 1 |

AMSEL-CT-R

Distribution List for Contract DAAB07-74-C-0272, Georgia Inst of Technology

NR. OF COPIES

Cdr, US Army Electronics Command
Fort Monmouth, NJ 07703

| | | | | | | | |
|---|---|---|---|---|---|---|---|
| 1 | AMSEL-NV-D | 1 | AMSEL-VL-D | 1 | AMSEL-MA-MP | 1 | AMSEL-PA |
| 1 | AMSEL-WL-D | 1 | AMSEL-CT-R | 1 | AMSEL-MS-TI | 1 | AMSEL-RD |
| 1 | AMSEL-NL-D | 1 | AMSEL-SI-CB | 1 | AMSEL-GG-RD | 1 | TDC-LNO |

This contract is supervised by Radar Technical Area, Combat Surveillance and Target Acquisition Laboratory, US Army Electronics Command, Fort Monmouth, New Jersey 07703. Tel: Eatontown, NJ, Area Code (201) 596-1407.